Design of electrodes for stimulation and recording

4

B. Howell, W.M. Grill
Duke University, Durham, NC, USA

4.1 Introduction

4.1.1 Neural stimulation and recording electrodes

Electrodes are electrical conductors made of a metal or polymer that electrically join metallic and nonmetallic conducting bodies. Throughout the nineteenth and early twentieth century, electrodes were primarily used to study electrochemical processes, make batteries, weld, and apply metal coatings to the surface of materials. However, with the advent of the microchip and microfabrication techniques in the past 50–60 years, electrodes have emerged as a promising technology for creating prosthetic devices that treat neurological disorders and restore function following injury to the nervous system.

Electrodes can be used either for stimulation or for recording. Stimulation electrodes inject charge into the neural tissue, the flow of charge (i.e., current) generates a distribution of electric potentials, and the extracellular potentials elicit a neural response by polarizing the membranes of electrically excitable cells residing in the tissue. Recording electrodes, on the other hand, do not inject charge, but rather monitor the electrical activity within the nervous system by measuring the electric potentials generated by neural elements (e.g., cells and axons) within the tissue.

4.1.2 Examples of neural prosthetic devices

Examples of devices that stimulate the central nervous system (CNS) include brain stimulation for treating motor symptoms in essential tremor and Parkinson's disease (Limousin, Speelman, Gielen, & Janssens, 1999; Montgomery, 1999); brain stimulation for treating epilepsy (Hodaie, Wennberg, Dostrovsky, & Lozano, 2002; Velasco, Velasco, & Velasco, 2001) and psychiatric disorders (Kuhn et al., 2010; Mayberg et al., 2005); brain stimulation (Coffey, 2001) and spinal cord stimulation (Cameron, 2004) for treating chronic pain; stimulation of the cochlea and brainstem for restoring hearing (Shannon, 2012); and stimulation of the retina and visual cortex for restoring vision (Rizzo & Wyatt, 1997). Further, examples of devices that stimulate the peripheral nervous system (PNS) include vagus nerve stimulation for treating epilepsy (Schachter & Saper, 1998) and depression (Sackeim et al., 2001), occipital nerve stimulation for the treatment of occipital neuralgia (Weiner & Reed, 1999), sacral nerve stimulation for treating bladder dysfunction (Jezernik, Craggs, Grill, Creasey, &

Implantable Neuroprostheses for Restoring Function. http://dx.doi.org/10.1016/B978-1-78242-101-6.00004-5

Rijkhoff, 2002), and stimulation of lower motor neurons to restore lost motor function (Peckham & Knutson, 2005).

Although less numerous, there are also devices that record activity from the CNS. These include brain–machine interfaces (BMIs) that use recordings of individual neurons in the cortex to control assistive devices that restore motor function in paralyzed individuals (Lebedev & Nicolelis, 2006) and devices that use recordings of local field potentials (LFPs) in cortical tissue to predict and subsequently prevent—through stimulation—the onset of seizures (Elger & Lehnertz, 1998).

Figure 4.1 shows examples of electrode designs that are currently used in neural prostheses. Electrodes used to stimulate the brain, spinal cord, and nerves are typically

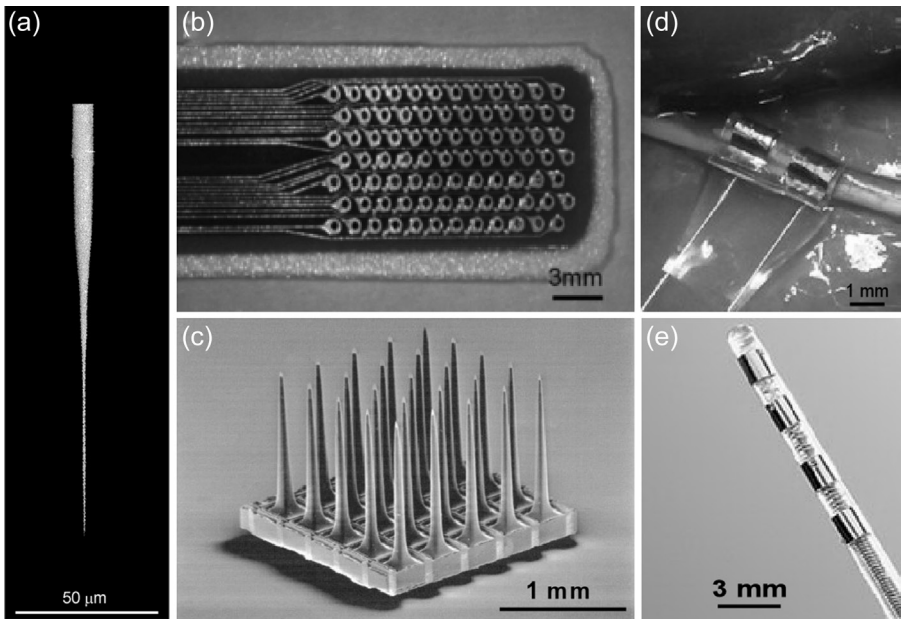

Figure 4.1 Examples of electrodes for neural stimulation and recording. (a) A carbon fiber-based microelectrode used for recording electrical activity from single neurons (units) in the nervous system *(adapted from Budai, 2010, Carbon-fiber based microelectrodes and microbiosensors)*. (b) An array of platinum electrodes on a flexible polyimide substrate used for retinal stimulation *(adapted from Cicione et al., 2012, Journal of Neural Engineering with Permission from IOP Science)*. (c) An array of silicon microelectrodes developed at the University of Utah *(adapted from Branner & Normann, 2000,* Brain Research Bulletin *with permission from Elsevier Science)* used for both stimulation and recording. Each electrode is ~80 μm wide at its base and tapers to an exposed sharpened tip. (d) A nerve cuff electrode, consisting of two platinum electrodes embedded in an insulating silicone substrate (*adapted from Foldes et al., 2011,* Journal of Neuroscience Methods *with permission from Elsevier Science*) that is used to record the electrical activity of nerves. (e) An array of four cylindrical platinum–iridium electrodes embedded within a polyurethane substrate (Lead Model 3387; Medtronic, Inc., Minneapolis, MN) used for deep brain stimulation (image from: http://professional.medtronic.com/pt/neuro/dbs-md/prod/dbs-lead-model-3387/#.VAZ5i_ldVBk). Similar designs are also used for spinal cord stimulation and cochlear stimulation.

made of a platinum and iridium (PtIr) alloy and have dimensions on the order of millimeters (Figure 4.1(d) and (e)). Smooth cylindrical surfaces are used to mitigate tissue damage from implantation; PtIr is used because of its biocompatibility and relatively large reversible charge injection capacity; but the choice of electrode dimensions is largely based on trial and error. Recording electrodes vary more in their shape, material composition, and size. Electrodes used to record single neurons are sharp tipped; made from biocompatible materials, such as stainless steel, tungsten, or PtIr; and have dimensions on the order of tens of micrometers (Figure 4.1(a) and (c)). Surface electrodes and implanted electrodes used to record from large volumes of tissue are typically planar, have dimensions on the order of millimeters, and are made of silver/silver chloride and PtIr, respectively.

4.1.3 Improving the performance of stimulation and recording electrodes

Neural prostheses have had substantial clinical success during the past two decades. For example, deep brain stimulation (DBS) of the subthalamic nucleus is more effective than the best medical management in treating the motor symptoms of Parkinson's disease (Kleiner-Fisman et al., 2006), and spinal cord stimulation (SCS) reduces pain (>50%) in individuals with chronic lower leg and back pain (Taylor, Desai, Rigoard, & Taylor, 2013). Despite these successes and the success of other emerging therapies, electrode design provides an opportunity to improve these therapies.

The median battery life of implantable stimulators used in DBS and SCS is ~3 (Okun et al., 2008) and ~4 (Bell, Kidd, & North, 1997) years, respectively. Because stimulation is typically administered continuously, multiple replacement surgeries are required in typical patients, and these are costly and obligate the patient to incur repeatedly the risks associated with surgery, including infection (Boviatsis, Stavrinou, Themistocleous, Kouyialis, & Sakas, 2010; Bronstein et al., 2011; Cameron, 2004) and hardware complications (Okun et al., 2005). Therefore, stimulation efficiency is one area that can be improved.

Another area that can be improved is stimulation selectivity. Suboptimal electrode placement is a common mode of failure in DBS (Ellis et al., 2008; Okun et al., 2008, 2005) and SCS (Cameron, 2004). In some cases, lead deviations preclude some or all potential clinical benefits (Bronstein et al., 2011; Ellis et al., 2008; Okun et al., 2008, 2005), and in others, misplacement generates adverse side effects from stimulation of nontarget regions (Cameron, 2004; Okun et al., 2008). Small lead misplacements can in some cases be overcome by altering the amplitude, duration, and frequency of the applied electrical waveform (Cameron, 2004; Kuncel & Grill, 2004); but larger misplacements require an additional surgery to reposition the lead (Ellis et al., 2008).

In addition to performance, the risks associated with implantation and residence of the electrode(s) must be considered. Implantation of an electrode displaces neural tissue, damaging blood vessels, ECM, and neurons and glia. The tissue responds to this insult and the chronic presence of electrode by altering the environment around the electrode, potentially leading to further loss of neurons (Polikov, Tresco, & Reichert, 2005). Because the performance of neural prostheses is dependent on the

long-term survival of the targeted neural elements, both stimulation and recording electrodes must be designed to mitigate the tissue response.

This review describes the fundamental principles of electrode design for neural stimulation and neural recording and how these principles can be used to advance the efficacy of neural prosthetic devices. In the first section, we cover the design of stimulation electrodes and how they can be made more efficient by consuming less power, more selective by reducing coactivation of nontarget elements, and less damaging during stimulation. In the following section, we cover recording electrodes and how they can be designed to be more selective in what neural signals they record, less prone to electrical noise, and less damaging within neural tissue. The review ends with a brief overview of prospective future directions in electrode design.

4.2 Stimulation electrodes

A stimulation electrode that is effective in activating neural elements satisfies three criterion: it is efficient, selective, and minimizes damage to the neural tissue. Efficient electrodes modulate (i.e., activate, inhibit, or block) the activity of neural elements, such as LNs or axons, using as little electrical energy as possible. Decreased energy consumption directly extends the lives of nonrechargeable batteries and indirectly extends the lives of rechargeable batteries by decreasing the number of recharge cycles, which in either case, reduces the cost and risks associated with battery replacement surgeries. Selective electrodes are able to target neural elements based on their size, orientation, or type, which reduces the sensitivity of clinical outcomes to (mal) positioning of the electrode. And electrodes that minimize damage to the neural tissue, from implantation and/or stimulation, will reduce risks associated with stimulation therapies.

4.2.1 Designing more efficient stimulating electrodes

Increasing stimulation efficiency requires decreasing the electrical energy required to modulate the activity of target neural elements. The instantaneous electrical power (P) transferred to the neural tissue is the product of the applied voltage (V) and applied current (I),

$$P = IV. \tag{4.1}$$

Electrical energy (E) is the time integral of P,

$$E = \int P \mathrm{d}t. \tag{4.2}$$

Therefore, E is reduced by decreasing the applied voltage and/or applied current that is used to modulate the activity of the target neural elements. Understanding how this can be accomplished, however, first requires understanding the electrical characteristics of the electrode, tissue, and target neural elements.

4.2.1.1 *Circuit representations of the electrode, tissue, and neural elements*

The electrode and connecting wires in current electrical stimulation devices are made of metal. Metals conduct electrons, whereas biological tissues conduct ions—such as sodium, potassium, and chloride—so an interface exists between the electrode and the tissue, known as the electrode–tissue interface (ETI), where charge changes form as it is transferred between the electrode and the tissue. Charge transfer can occur in one of three ways: it can be non-Faradaic (capacitive/indirect), where equal and opposite charges in the electrode and tissue are redistributed via Columbic forces; Faradaic (or direct), where electrons are transferred between the electrode and the tissue via electrochemical (i.e., oxidation and reduction) reactions; or a combination of both direct and indirect charge transfer, such as the electrochemical generation of (specific and nonspecific) adsorbable species (Figure 4.2(a)).

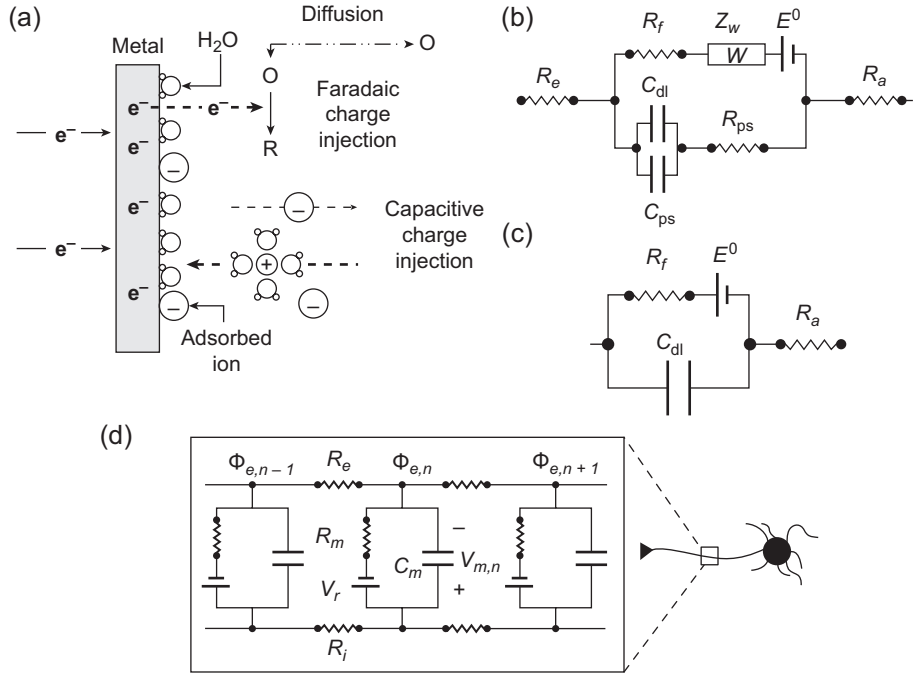

Figure 4.2 Circuit representations of an electrode in tissue and a neural element. (a) The electrode–tissue interface (ETI) and possible modes of charge injection, including Faradaic charge injection, non-Faradaic/capacitive charge injection, and charge injection via the generation and (specific and nonspecific) adsorption of ions. (b) The Timmer equivalent circuit representation of the electrode, ETI, and tissue. R_e is the resistance of the metal electrode, R_f is the Faradaic resistance, Z_w is the Warburg element, C_{dl} is the double-layer capacitance, C_{ps} and R_{ps} are the pseudocapacitance and resistance, respectively, R_a is the access resistance, and E^0 is the standard electrode potential. (c) The Randles equivalent circuit that results when R_e, Z_w, C_{ps}, and R_{ps} are ignored from (b). (d) A lumped circuit representation of a patch of membrane of a neuron. R_m and C_m are the membrane resistance and membrane capacitance, respectively; V_m is the membrane potential; V_r is the resting membrane potential; R_i and R_e are the intracellular/axoplasmic and extracellular resistances, respectively; Φ_e is the external potential; and n denotes the index of the compartment.

Given the above, we can build what is known as the Timmer equivalent circuit representation of an electrode in tissue (Figure 4.2(b)). Electrons flow freely through the electrode and connecting wires, so they are modeled as a single conductor with an ohmic resistance (R_E). Indirect charge transfer at the ETI is modeled with two parallel-plate capacitors: a double-layer capacitor (C_{dl}) that accounts for charge redistribution and a pseudo-capacitor (C_{ps}) in series with a charge transfer resistance (R_{ps}) that accounts for ion adsorption and the electrochemical reactions that give rise to the adsorbed species, respectively. Direct charge transfer is modeled using a series combination of a Faradaic resistance (R_f) that accounts for the transfer of electrons in electrochemical reactions, a Warburg element (Z_W) that accounts for mass transfer (diffusion) limitation in these reactions, and a battery (E^0) that accounts for the electromotive force at equilibrium when no current is applied. Beyond the electrode and ETI, ions flow freely, so the tissue is also modeled as a single conductor with an ohmic resistance known as the access resistance (R_a).

In some electrical stimulation therapies, such as DBS and SCS, charge transfer occurs in a short enough time scale that both diffusion limitations and adsorption are negligible, and the electrical loads presented by the stimulation electrode and connecting wires are small compared to the loads presented by the ETI and tissue. In these cases, R_E, Z_W, C_{ps}, and R_{ps} can be ignored, yielding what is known as the three-element Randles equivalent circuit (Figure 4.2(c)).

The neural elements targeted in electrical stimulation therapies can also be modeled by a distributed network of electrical circuit elements. Neural elements include LNs, consisting of a cell body (soma), dendrites, axon, and axon terminal; and the axons of distal neurons that pass by or terminate in the target brain region. Axons and dendrites are much longer than they are wide and azimuthally symmetric about their longitudinal axis, so they are typically modeled as a one-dimensional cable of cylindrical membrane compartments (Figure 4.2(d)). The soma, although spherical, can also be approximated as a series of cylindrical compartments, and the flow of charge through the neuron can be described with a partial differential equation known as the Cable equation:

$$C_m \frac{\mathrm{d}V_{m,n}}{\mathrm{d}t} + \frac{(V_{m,n} - V_r)}{R_m} - \frac{\delta^2 V_{m,n}}{R_i} = \frac{\delta^2 \Phi_{e,n}}{R_i}. \tag{4.3}$$

R_m and C_m are the membrane resistance and membrane capacitance, respectively, V_m is the membrane potential, V_r is the resting membrane potential, R_i is the intracellular/axoplasmic resistance between compartments, Φ_e is the external potential on the surface of the membrane, δ is the centered difference operator, and n denotes the index of the compartment.

The Randles circuit and Cable equation are used in the following sections to determine how one can alter the design of the electrode so that the energy transferred during stimulation is reduced.

4.2.1.2 Decreasing the electrode impedance

The efficiency of a stimulation electrode can be increased by decreasing the electrical load, or impedance, driven by the stimulator (Z_e). Reducing Z_e increases the amount of

current injected into the tissue per applied volt, which translates into less voltage being required to supply the critical amount of current (i.e., the threshold current) necessary to generate a distribution of potentials whose magnitude is large enough to evoke a neural response. Recall, Z_e includes the impedances of the connecting wires, electrode, ETI, and tissue (Figure 4.2(b)); and for typical electrical stimulation therapies, Z_e is dominated by the impedances of the ETI and tissue—namely C_{dl}, R_f, and R_a (Figure 4.2c). Since resistors have an impedance that is proportional to their resistance, and since capacitors have an impedance that is inversely proportional to their capacitance, Z_e can be decreased by increasing C_{dl}, decreasing R_f, and/or decreasing R_a.

C_{dl} can be modeled as a parallel-plate capacitor with a capacitance, $C = \varepsilon_0 \varepsilon_r A_e / d$, where ε_0 is the vacuum permittivity, ε_r is the relative permittivity of the interface, A_e is the 3D (or microscopic) area of overlap between the electrode and the tissue, and d is the thickness of the interface. With this, we see that one way to increase C_{dl} is to roughen the electrode surface at the microscopic level, markedly increasing A_e, while leaving the 2D (geometric) surface area (A) unchanged. Note, A_e is distinguished from A because the former describes changes in the electrode texture, while the latter describes changes in the electrode dimensions. For example, electrical deposition of dissolved platinum (Pt) onto Pt and titanium (Ti) can increase A_e up to 280 and 410 times, respectively, and vapor deposition of titanium nitride (TiN) onto Pt and Ti can increase A_e up to 1100 and 580 times, respectively (Norlin, Pan, & Leygraf, 2002).

C_{dl} can also be increased by coating the surface of the electrode with a thin dielectric material. Coating the electrode with a dielectric increases the ε_r of the ETI, and making the dielectric as thin as possible minimizes the accompanying increase in d. Since the dielectric prevents direct charge transfer, electrodes that use this approach are known as capacitive electrodes. Tantalum (Ta) and TiN electrodes are two types of capacitive electrodes that have been studied for neural stimulation. At positive (i.e., anodic) stimulation voltages, oxidation of Ta produces Ta pentoxide (Ta_2O_5) with an ε_r of 25, and oxidation of TiN produces the rutile form of Ti dioxide (TiO_2) with an ε_r of 100 (Rose, Kelliher, & Robblee, 1985). Compared to Ta_2O_5, TiO_2 is more porous and therefore more susceptible to undesirable irreversible reduction–oxidation (redox) reactions, such as the hydrolysis of water (Rose et al., 1985). However, compared to TiN electrodes, Ta electrodes have a smaller reversible charge injection capacity, are less amenable to surface roughening, and require relatively high bias voltages (>4 V) between stimulation pulses to maintain the formation of Ta_2O_5. Therefore, TiN electrodes are more extensively used for electrical stimulation (Cogan, 2008).

The dependence of R_f on the geometry and material properties of the electrode is not obvious. The relationship between the potential drop across R_f, often referred to as the overpotential (η), and the Faradaic current (I_η) through the ETI is nonlinear and generally cannot be expressed in a closed-form solution. Yet, one can still achieve a qualitative understanding of how to alter R_f by examining basic principles. Consider a first-order redox reaction. According to the law of mass action, the current I_η that flows from such a reaction can be expressed as

$$I_\eta = nFA_e k_x C_x, \tag{4.4}$$

where n is the number of electrons transferred, F is the Faraday constant, k_x is the rate constant of the reaction (in s^{-1}), and C_x is the surface concentration of the reacting species (in mol/m^2). For simple reactions, where the external distribution has a negligible effect on the reacting species, collision theory says that k_x has an exponential dependence on η. Implicit differentiation of Eqn (4.4) with η as the dependent variable yields an expression for $d\eta/dI_\eta = R_f$ that is inversely proportional to A_e. Therefore, surface roughening techniques that increase A_e are also able to decrease Z_e by decreasing R_f.

Another way to decrease R_f is to apply what is known as a Faradaic electric coating. Faradaic coatings work by introducing a redox couple with a relatively large kinetic facility so that a greater amount of I_η can be generated per change in η. One of the most widely used Faradaic coatings for electrical stimulation is a hydrated film of iridium (Ir) oxide. Ir oxide can be rapidly and reversibly oxidized or reduced between two oxidative states, Ir^{3+} and Ir^{4+}. Because the reactants remain bound to the electrode surface, Faradaic coatings impart what is referred to as pseudo-capacitance. Pseudo-capacitance is advantageous, because like capacitance, it allows reversible charge injection, which minimizes the probability of damage to the electrode and tissue. For example, Pt electrodes can reversibly inject up to 0.3 mC/cm^2, whereas PtIr electrodes with an Ir oxide coating have the ability to inject up to ±1 and ±2 mC/cm^2 for cathodic and anodic stimulation, respectively (Cogan, 2008).

We discuss the effects of R_a by considering a spherical electrode with a radius of r_a that resides in an infinite conducting medium whose resistivity, ρ, is homogeneous (i.e., the same at all locations) and isotropic (i.e., the same in all directions). In this case, it can be shown that $R_a = \rho/4\pi r_a$. Of course, different geometries would yield different expressions for R_a, but this equation illustrates that R_a is inversely related to the macroscopic dimensions of the electrode. Thus, one way to reduce R_a is by increasing the 2D geometric surface area, A, of an electrode.

In the above example, the current density ($\vec{J}$) on the surface of a spherical electrode is uniform, but the same is not true for electrodes that are inlaid in an insulating substrate (Figure 4.1(b)–(e)). In these cases, $\vec{J}$ is largest on the edges (or perimeter) of the electrode where the metal and insulator meet, so R_a can also be reduced by increasing the electrode perimeter (Pendekanti & Henriquez, 1996; Wei & Grill, 2005). These "edge effects," however, are not as pronounced as the effect of increasing A (Howell & Grill, 2014). For example, quantitative measurements have revealed that doubling the perimeter of an array of cylindrical electrodes decreased its impedance by ~17%, whereas doubling the area (or coverage) of the cylindrical electrode array decreased its impedance by ~30% (Pendekanti & Henriquez, 1996).

4.2.1.3 Altering the driving force for neural activation

Reducing Z_e is not the only means to increase efficiency. Recall the cable equation (Eqn (4.3)), whose right-hand side (or forcing function) represents the source driving polarization of the neural membrane during electrical stimulation (Rattay, 1986). Since the source term is proportional to the second centered spatial difference of the extracellular potentials ($\delta^2\Phi$), stimulation efficiency can also be increased or decreased by altering $\delta^2\Phi$. This is known as field shaping.

Consider a point source electrode in an infinite conducting medium with homogeneous and isotropic ϱ. The potentials generated by the point source are described by

$$\Phi(r) = \frac{\rho I_e}{4\pi r}, \tag{4.5}$$

where I_e is the source current and r is the radial distance from the source. Equation (4.5) is spherically symmetric, so $\delta^2\Phi$ evaluated between any three connective points in space (e.g., between three adjacent nodes of Ranvier of an axon) is independent of orientation, as long as those three points have the same corresponding r_e (Figure 4.3). Therefore, $\delta^2\Phi$ of electrodes that resemble a point source, such as spherical electrodes and microelectrodes with an exposed tip, will depend on the applied current and distance but not direction or orientation.

It follows that if an electrode is not spherical, then it will produce an asymmetric potential distribution whose corresponding $\delta^2\Phi$ depends on direction. Consider a finite line source in an infinite medium with a homogeneous and isotropic ρ. The potentials generated by a line source in this case are described by

$$\Phi(x, y, z) = \frac{\rho\lambda}{4\pi} \ln \left\{ \frac{\sqrt{(z-L/2)^2 + (x-x_e)^2 + (y-y_e)^2} + (z-L/2)}{\sqrt{(z+L/2)^2 + (x-x_e)^2 + (y-y_e)^2} - (z+L/2)} \right\}, \tag{4.6}$$

where λ is the linear current density (in A/m), L is the length of line source, and x_e and y_e are the Cartesian coordinates of the midpoint of the line source with respect to the origin. Perpendicular to the long axis of the line source, the potentials have a shape that is similar to that of a point source, but parallel to its long axis, the potentials are flattened, leading to a marked reduction in $\delta^2\Phi$ (Figure 4.3). By comparing Eqn (4.5) when $I_e = -1$ mA to Eqn (4.6) when $\lambda = -1/3$ mA/mm and $L = 6$ mm, we see that the line source, despite applying twice as much current, generates a $\delta^2\Phi$ that is comparable to or less than the $\delta^2\Phi$ of the point source, depending on the orientation (Figure 4.3). Therefore, changes in efficiency that result from field shaping can be similar to or greater than changes in efficiency that result from altering Z_e.

Field shaping can also be achieved by steering current between two or more electrodes in a multipolar configuration. The most basic multipolar configuration is a bipole, which consists of a source (anode) and a sink (cathode). Let us return to our previous example of a point source in an infinite conducting medium with a homogeneous and isotropic ρ. If we extend this example by adding a point sink, then the potentials generated by the bipolar pair can be expressed as

$$\Phi = \frac{\rho I_e}{4\pi} \left(\frac{1}{r_+} - \frac{1}{r_-} \right), \tag{4.7}$$

where r_+ and r_- are the distances to the source and the sink, respectively. Equation (4.7) changes sign: the potentials are positive when $r_+ < r_-$, zero when $r_+ = r_-$, and negative

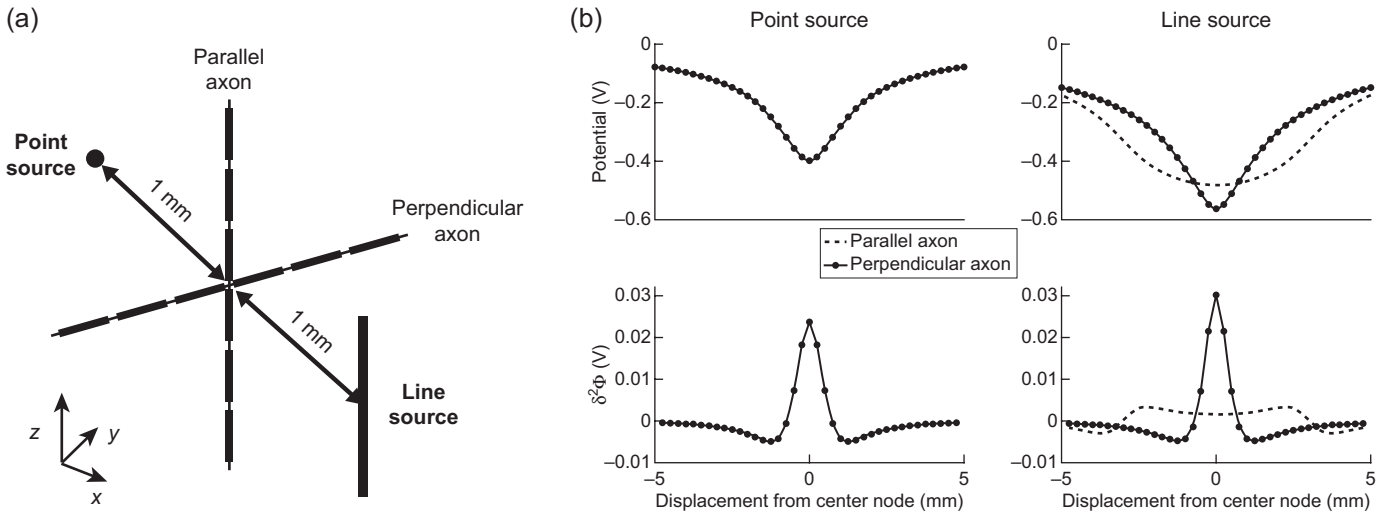

Figure 4.3 The effect of electrode geometry on the source driving neural polarization. (a) A point source (PS) and a line source (LS) extending in the z direction are used separately to stimulate two axons in an infinite conducting medium with a homogeneous and isotropic conductivity of 0.2 S/m, equal to that of gray matter (Gabriel, Peyman, & Grant, 2009). The axons are displaced 1 mm from the PS and 1 mm from the midpoint of the LS, and in both cases, the axons are orientated parallel and perpendicular to the z-axis. (b) The potentials (top) and the centered second difference of the potentials ($\delta^2\Phi$, bottom) generated at the nodes of the two axons when the PS (left) and LS (right) inject 1 and 2 mA, respectively.

when $r_+ > r_-$. Therefore, with a bipole, the magnitude of the difference in potentials between two points, $|\Delta\Phi_n| = |\Phi_n - \Phi_{n+1}|$, is bounded between 0 and $|\Phi_n| + |\Phi_{n+1}|$. To compare, a monopole (Eqn (4.5)) has a $|\Delta\Phi_n|$ that is bounded between 0 and the maximum of $|\Phi_n|$ and $|\Phi_{n+1}|$, so the $\Delta\Phi$ of a bipole can be greater than the $\Delta\Phi$ of a monopole.

The goal, however, is not to increase $\Delta\Phi_n$ but $\delta^2\Phi_n$. Expanding $\delta^2\Phi_n$ in terms of its backward difference $(\Phi_n - \Phi_{n-1})$ and its forward difference $(\Phi_{n+1} - \Phi_n)$ yields the following expression: $\delta^2\Phi_n = (\Phi_{n+1} - \Phi_n) - (\Phi_n - \Phi_{n-1})$. In this form, we see that $\delta^2\Phi_n$ can be increased by using not one but two bipoles, opposite in orientation, that share a common sink. This is referred to as a tripole (Figure 4.4(a)). The first and second bipole increase the magnitude of $(\Phi_{n+1} - \Phi_n)$ and $(\Phi_n - \Phi_{n-1})$, respectively, and because the bipoles are in opposite orientations, the two differences are of opposite sign. As a result, a tripole generates a $\delta^2\Phi_n$ that can be as large as $|\Phi_{n+1} - \Phi_n| + |\Phi_n - \Phi_{n-1}|$, which is greater than the maximum possible $\delta^2\Phi_n$ generated by a monopole applying the same amount of current (Figure 4.4(b)).

4.2.2 Designing more selective stimulation electrodes

Efficacy also requires that an electrode be able to activate selectively specific elements of the nervous system. In SCS, it is hypothesized that the therapeutic effect is achieved when axons in the dorsal column (DC) of the spinal cord are activated without coactivation of nearby afferents in the dorsal root (DR) (Holsheimer, 2002; Struijk, Holsheimer, & Boom, 1993). In retinal prostheses, the quality of visual perception is thought to depend on the ability to activate nearby retinal ganglion cells (RGCs) without coactivating passing axons of distal RGCs (Rattay & Resatz, 2004; Schiefer & Grill, 2006). Also, DBS clinical studies have shown that lead deviations as small as 2–3 mm can preclude some or all clinical benefits (Bronstein et al., 2011; Ellis et al., 2008; Okun et al., 2008, 2005), and in some cases generate adverse side effects (Okun et al., 2008). Increased selectivity is achieved by activating neural elements based on their orientation, location, size, and/or type.

4.2.2.1 Activation based on orientation

Selective activation of neural elements based on their orientation is achieved by shaping the potential distribution so that $\delta^2\Phi$ in one orientation is larger than $\delta^2\Phi$ in other nontarget orientations. One way to accomplish this is by altering electrode geometry. Consider a cylindrical electrode whose axis lies in the z direction. Elongation of the cylinder by increasing its height causes the current density $\vec{J}$ to become more uniform along its axis. If we assume that the electric field ($\vec{E}$) is both static ($\vec{E} = -\nabla\Phi$) and linear ($\vec{J} \cdot \rho = \vec{E}$), which is a reasonable approximation for many electrical stimulation therapies, then as $\vec{J}$ in the z direction becomes more uniform, $\nabla \cdot \vec{J}$ in the z direction approaches 0. This means $\delta^2\Phi$ is reduced along the axis of the elongated electrode (Figure 4.3), lowering the source driving polarization of parallel elements so that perpendicular elements are activated first.

Orientation-dependent activation of neural elements can also be achieved using a multipolar configuration, such as a tripole. Recall from Section 4.2.1.3 that a tripole

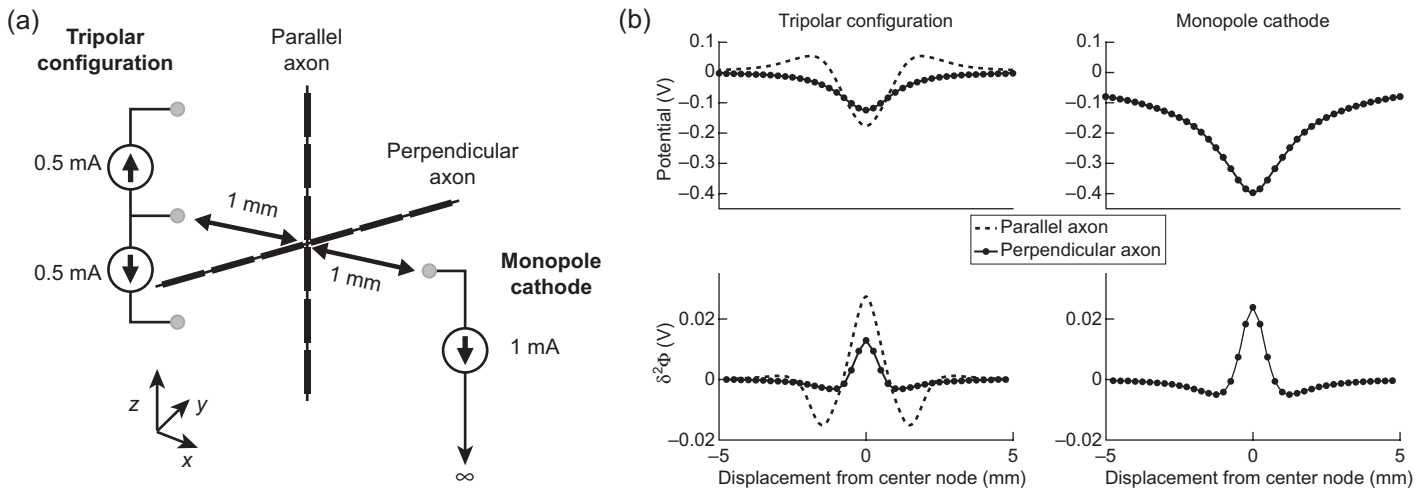

Figure 4.4 Current steering and its effects on the source driving neural polarization. (a) A point source (PS) and a tripole, which consists of two oppositely oriented bipoles along the z-axis that share a common sink, are used individually to stimulate two axons placed in an infinite conducting medium with a homogeneous and isotropic conductivity of 0.2 S/m, equal to that of gray matter (Gabriel et al., 2009). The axons are displaced 1 mm from the PS and 1 mm from the sink of the tripole. In both cases, the axons are oriented parallel and perpendicular to the z-axis. (b) The potentials (top) and the centered second difference of the potentials ($\delta^2\Phi$, bottom) generated at the nodes of the two axons when the tripole (left) and PS (right) release 1 mA of current.

consisting of two bipoles in opposite orientations increases $\delta^2\Phi$. Parallel to the displacement vector ($\vec{d}$) that points from the sink to the source, the potentials change sign, but perpendicular to $\vec{d}$, the sign of the potentials does not change. This means the ability of a tripole to alter $\delta^2\Phi$ is maximal and minimal in directions that are parallel and perpendicular to $\vec{d}$, respectively (see Figure 4.4). Therefore, tripoles—and potentially other multipolar configurations—can activate elements parallel to the electrode at lower stimulation thresholds than elements perpendicular to the electrodes.

Although the performance of tripoles and elongated electrodes has not been extensively tested in a clinical setting, a number of modeling studies have looked at potential applications of these geometries. In SCS, tripoles are predicted to perform better than bipoles and monopoles in activating the therapeutic targets, the DC fibers, over the undesirable targets, the DR fibers (Holsheimer, 1998; Holsheimer, Struijk, & Wesselink, 1998; Manola & Holsheimer, 2004); and in retinal stimulation therapies, elongated arrays of electrodes are expected to have a high degree of selectivity in activating local RGCs over the axons of distal RGCs that pass parallel to the array (Rattay & Resatz, 2004).

4.2.2.2 Activation based on spatial location

The potentials generated by an electrode decrease in magnitude with increasing distance. In general, $\delta^2\Phi$ declines as the magnitude of the potentials declines, so the ability of an electrode to activate elements near its surface selectivity depends on how rapidly the potentials decay. In some cases, for example, when targeting individual fascicles within a nerve, the closest elements can be selectively activated by using the contact(s) closest to the target population (Kent & Grill, 2013; Sweeney, Ksienski, & Mortimer, 1990). However, in other cases, such as brain stimulation, where the target and nontarget population can be in close proximity, other techniques are required.

Multipolar configurations with relatively small interelectrode spacings can be used to increase the spatial selectivity of an electrode. For example, when the distance to a bipole is much greater than the distance between the source and sink, the potentials decline proportional to $\sim 1/r^2$. To compare, the potentials of a point source decay proportional to $1/r$ (Eqn (4.5)), so electrode pairs that resemble a bipole have better spatial selectivity than a single electrode. Higher order multipoles with small interelectrode spacings, such as a tripole, have potentials that decay $\sim 1/r^3$, so as a general principle, the spatial selectivity of a multipole increases with its order.

Other than SCS, there are very few applications that currently use multipolar configurations. Yet, this may change in the future, as multipolar configurations are being considered for better targeting in DBS, especially in cases where the electrode is suboptimally placed (Keane, Deyo, Abosch, Bajwa, & Johnson, 2012).

4.2.2.3 Activation based on size

In the PNS, the natural recruitment order of motor units (defined as a motor neuron and its innervated muscle fibers) is from smallest to largest. However, in external electrical stimulation, $\delta^2\Phi$ increases with increasing fiber diameter (D), and the recruitment order of motor axons is reversed. The largest motor axons are fast glycolytic, type II fibers,

which generate large forces and fatigue easily, so in therapies that aim to restore lost motor function, such as functional electrical stimulation, evoking dexterous movements and sustained activation without fatigue is a challenge (Peckham & Knutson, 2005).

One design for restoring the natural recruitment order is a tripolar electrode in an anode–cathode–anode configuration. A tripole generates a $\delta^2\Phi$ that is maximally positive and thereby depolarizing closest to the cathode (Figure 4.4(b)), so when a motor axon is activated, the action potential (AP) initiates in the nodes of the Ranvier (NoR) most proximal to the cathode. At the same time, the flanking anodes (Figure 4.4(b)) hyperpolarize distal NoRs, and at large enough stimulation amplitudes, the AP can be blocked, starting with the largest D axons. Blocking, however, requires a trapezoidal waveform with a relatively long duration on the order of 1 ms; the leading edge and plateau phases must last long enough to block the propagating AP (~350 μs), and the trailing edge phase must decline over a long enough period (~600 μs) that anodic block excitation does not occur on termination of the blocking pulse (Fang & Mortimer, 1991a, b).

Another design for restoring the natural recruitment order is a longitudinal array of five or more electrodes in an alternating source–sink configuration (Lertmanorat & Durand, 2004; Lertmanorat, Gustafson, & Durand, 2006). An alternating array produces a sinusoidal distribution of potentials. Activation of myelinated motor axons depends on $\delta^2\Phi$ between the NoR and the intermodal length (INL) between nodes is linearly proportional to D (Murray & Blakemore, 1980). Thus, only axons with INL > the center-to-center interelectrode spacing of the electrode will spatially alias the source term, resulting in a reduced $\delta^2\Phi$ for large D axons. This technique works independent of the pulse width of stimulation, so unlike a tripolar electrode, it can be used for relatively small pulse widths of <500 μs.

4.2.2.4 *Activation of specific neural elements*

There is growing evidence in brain stimulation therapies showing that the therapeutic targets are local afferent fibers. High-frequency DBS of cerebellar afferents in the Vim is predicted to mask tremor-associated burst activity in essential tremor (Birdno et al., 2012); high-frequency stimulation of cortical afferents in the subthalamic nucleus (STN) reduces parkinsonian symptoms in rats (Gradinaru, Mogri, Thompson, Henderson, & Deisseroth, 2009); and tonic stimulation of afferents in the nucleus accumbens reduces depressive symptoms in mice (Chaudhury et al., 2012). For that reason, neural prostheses can be made more effective by designing electrodes that selectively activate terminating axons (TAs) over other neural elements, such as axons of passage (AOPs) or local neurons (LNs).

The source driving membrane polarization at the terminal of TA is not proportional to $\delta^2\Phi$ but rather proportional to $\Delta\Phi$, so electrodes that can markedly increase $\Delta\Phi$ have the ability to selectively target TAs. The simplest example of this is a bipole (Figure 4.5(a)). A bipole has the ability to increase $\Delta\Phi$ (Section 4.2.1.3), and the ability to increase $\Delta\Phi$ is maximal in directions that are parallel to $\vec{d}$ (Section 4.2.2.1). Hence, a bipolar electrode activates TAs at lower stimulation thresholds than passing axons because it generates a $\Delta\Phi$ parallel to $\vec{d}$ that is greater than the maximum $\delta^2\Phi$ in directions that are parallel and perpendicular to $\vec{d}$ (Figure 4.5(b)).

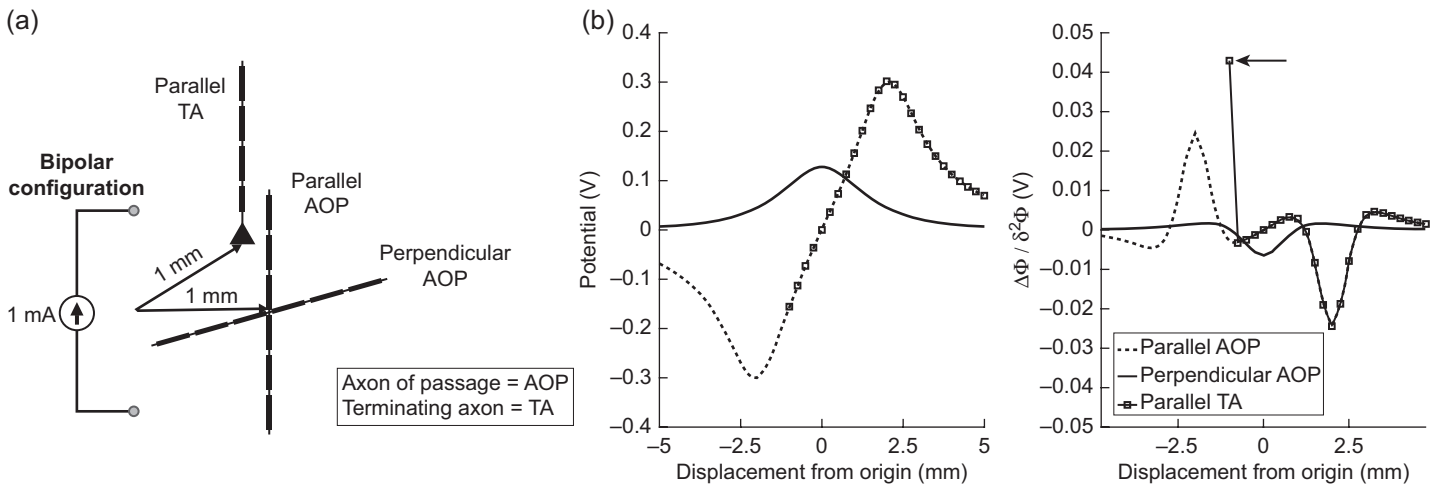

Figure 4.5 Selective activation of terminating axons at lower thresholds than axons of passage. (a) Two point source electrodes in a bipolar configuration are used to stimulate a parallel terminating axon (TA), a parallel axon of passage (AOP), and a perpendicular AOP in an infinite medium of gray matter (0.2 S/m) (Gabriel et al., 2009). The neural elements are positioned such that the center nodes of the parallel and perpendicular AOP and the terminal of the TA are all 1 mm from the center of the bipolar electrode pair. (b) The potentials (left) and the centered second difference of the potentials ($\delta^2\Phi$, right) at the nodes of the neural elements being stimulated. The arrow indicates the first difference of the potentials ($\Delta\Phi$) at the terminal of the TA.

Selective activation of TAs over AOPs and LNs is the objective when the electrode is downstream of the target neuron population. However, in cases where the electrode is implanted upstream, where the axons of the therapeutic targets originate, then the objective shifts to activation of LNs at lower stimulation thresholds than AOPs and/or TAs. Techniques for selectively activating LNs fall outside the scope of electrode design, but a discussion of these techniques can be found in Schiefer and Grill (2006), McIntyre and Grill (2000), and Wang, Millard, Zheng, and Stanley (2012).

4.2.3 Designing nondamaging stimulation electrodes

Regardless of how efficient and selective an electrode design is, to be effective it must also minimize damage to the nervous tissue. Damage to the neural tissue can occur passively, due to implantation and residence of the electrode within the tissue, or dynamically, as a result of stimulation. Therefore, designing electrodes that minimize tissue damage requires an understanding of the "passive" and "dynamic" tissue responses.

The passive tissue response includes the inflammatory and immune response to injuries during implantation and the presence of the electrode, as well as cellular responses to mechanical stresses that arise from relative movement of the electrode and tissue. Since this response pertains to both stimulation and recording electrodes, it will be covered in Section 4.3. The dynamic response includes changes or damage to the tissue that can arise from heat generation, electrochemical reactions that occur during charge injection, and/or nonphysiological activation of neurons; and because it is a product of passing current through the electrode(s), it pertains only to stimulation electrodes.

In Section 4.2.3, we cover the origins of the dynamic tissue response and how stimulation electrodes can be designed to mitigate this response. Polarization refers to any combination of stimulation parameters (amplitude, pulse width, and frequency), but our focus in on the range of parameters typically used for electrical stimulation. This includes amplitudes between 0 and 10.5 V and between 0 and 6 mA for voltage-regulated stimulation and current-regulated stimulation, respectively, pulse widths between 60 and 1000 μs, and frequencies between 1 and 5000 Hz (Table 4.1).

4.2.3.1 Mitigating heat generation

The electrode is a source of heat energy when passing current. In retinal prostheses, heat generation is predicted to increase temperatures 0.8 °C at the surface of the implant and 0.16–0.26 °C in the surrounding vitreous cavity (Gosalia, Weiland, Humayun, & Lazzi, 2004), and in DBS, temperatures are predicted to increase as much as 1 °C in the surrounding tissue at high stimulation settings (10 V, 185 Hz, 210 μs) (Elwassif, Datta, Rahman, & Bikson, 2012, Elwassif, Kong, Vazquez, & Bikson, 2006). Animal studies looking at the effects of temperature on brain tissue show that some neuronal death (~6%) occurs after 60 min at 40.5 °C and blood–brain barrier breakdown occurs after 60 min at 42 °C (Goldstein, Dewhirst, Repacholi, &

Table 4.1 Stimulation parameters approved for electrical stimulation therapies

Therapy		Amplitudes[b] (V/mA)	Pulse widths (μs)	Frequencies (Hz)
Central nervous system	Deep brain stimulation (Kuncel & Grill, 2004)	0–10.5 V (1–5 V)[a]	60–450 (60–210)[a]	2–185 (130–185)[a]
	Spinal cord stimulation (Alo, Yland, Kramer, Charnov, & Redko, 1998)	0–10.5 V	60–1000 (80–500)[a]	2–1200 (17–750)[a]
Peripheral nervous system	Vagal nerve stimulation	0–3.5 mA	130–1000	1–30
	Gastric nerve stimulation	0.5 mA	330	14
	Vagus nerve block	1–6 mA	100	5000

[a]Stimulation parameters typically used by patients.
[b]Amplitudes in volts (V) and milliamps (mA) represent voltage-regulated stimulation and current-regulated stimulation, respectively.

Kheifets, 2003). The American Association of Medical Instrumentation recommends that medical implants do not exceed temperature increases of 1–2 °C, but there is still a paucity of data on the long-term effects of small temperature increases on brain tissue.

Heat generation during electrical stimulation can be mitigated by distributing the thermal load. One approach is to increase the dimensions of the electrode. A larger electrode has a smaller power density (watts/unit area), which is proportional to the rate of change in the temperature (Pennes, 1948), so temperature increases are reduced, allowing heat loss due to perfusion to better compensate for the heat generated by the electrode. Increasing the electrode dimensions is advantageous because it can be more rapidly translated into clinical use, as it uses existing materials, but disadvantageous because larger electrodes may damage more tissue on implantation.

A second approach is to increase the thermal conductivity (W/°C) of the insulating substrate holding the electrode(s). Modifying the insulator with a material that has a relatively high thermal conductivity and low electrical conductivity (e.g., diamond, diamond-like carbon, and alumina ceramics) distributes the thermal load over the electrode shaft, decreasing the power density. For example, the thermal conductivity of the polyurethane insulator used in DBS and SCS (0.026 W/°C) is three orders of magnitude less than the thermal conductivity of the PtIr stimulation electrodes

(31 W/°C) (Elwassif et al., 2012). Increasing the thermal conductivity of the insulator 3–5 orders of magnitude reduces temperatures increases by approximately 35% and 72%, respectively (Elwassif et al., 2012).

4.2.3.2 Nondamaging charge transfer

Charge transfer at the ETI can lead to irreversible redox reactions that damage the electrode and tissue. Undesirable reactions include the reduction (electrolysis) of water and the oxidation (corrosion) and reduction (dissolution) of the metal electrode. It is for this reason that electrode designs with large reversible charge storage capacities (RCSC) are desirable.

Electrodes that transfer charge in a capacitive manner naturally have a large RCSC. For example, TiN electrodes (Section 4.2.1.2) have a maximum RCSC of ~1 mC/cm^2, which is one to two orders of magnitude greater than the RCSC of noble metals, such as Pt and PtIr (Cogan, 2008). Achieving such a large RCSC, however, requires a relatively high bias voltage (>4 V) in the period between stimulation pulses, which reduces stimulation efficiency.

An alternative solution to a capacitor electrode is an electrode that has pseudo-capacitance—that is, the ability to inject charge reversibly via redox reactions. Coated PtIr electrodes (Section 4.2.1.2) can inject up to 1 and 2 mC/cm^2 for cathodic stimulation and anodic stimulation, respectively (Merrill, Bikson, & Jefferys, 2005), so noble metals with Faradaic coatings are strong candidates for safe charge transfer.

In addition to irreversible redox reactions, tissue damage may also arise from stimulation-induced neural excitation, as persistent activation is an unnatural state for most neurons. One proposed mechanism for stimulation-induced neural injury is exitotoxicity. In exitotoxicity, excessive release of the neurotransmitter glutamate leads to persistent activation of ionotropic NMDA receptors on postsynaptic neurons and calcium ion (Ca^{2+}) flow into the cell, and the resultant pathologic levels of Ca^{2+} trigger the death of the neuron—via apoptosis. Because exitotoxicity is only one of a few proposed mechanisms for stimulation-induced neural injury, it still remains unclear what exactly leads to neuron injury. Regardless, the degree of injury is related to the charge density and the charge per phase of stimulation pulse (Mccreery, Agnew, Yuen, & Bullara, 1990), and models have been proposed to help delineate what levels of these factors are damaging to the neural tissue (Shannon, 1992). Thus, the electrode geometry and stimulation parameters should be chosen such that the charge density and charge per phase are nondamaging.

4.3 Recording electrodes

The flow of ions across the membrane of an electrically excitable cell generates a distribution of potentials in the extracellular space that can be recorded with an electrode. The spatiotemporal characteristics of the potentials depend on the cellular source of the transmembrane current, so a wide spectrum of signals exists: potentials recorded from neurons in the brain are referred to as an electroencephalogram

when recorded from the scalp and as LFPs (many cells) or single unit activity (one cell) when recorded from within the brain; and potentials recorded from axons in the CNS and PNS are referred to as an electroneurogram (ENG), in general, and more specifically as an compound action potential when the electrically activity is synchronized.

A recording electrode must satisfy three design criteria to be effective. First, a recording electrode must discriminate the target neural signal, both spatially and temporally, from nontarget neural signals. In some cases, the ability to discriminate the neural signal depends primarily on the proximity of the electrode to the cellular source, but in other cases (e.g., discrimination of a single unit), the geometry of the electrode is also important. Second, the recording electrode must minimize both intrinsic and extrinsic forms of electrical noise so that the target signal can be recorded with a high signal to noise ratio (SNR). Third, a recording electrode should produce minimal tissue damage from the implantation and residence of the electrode.

4.3.1 Discrimination of the target neural signal

The electric potentials generated in a volume of tissue by biological current sources and sinks can be discriminated based on spatial and temporal characteristics. Spatial discrimination is achieved by selecting the appropriate location, geometry, configuration, and material of the electrode based on the signal properties, while temporal discrimination is achieved through filtering (or signal processing) of the signal based on its amplitude or spectral properties. Because the latter does not depend on the electrode design, it will be covered only briefly.

4.3.1.1 Spatial discrimination

The reciprocity theorem, derived from Green's theorem in classical electromagnetism (Plonsey, 1963), can be used to understand how an electrode spatially discriminates electric signals arising from neural sources. Consider an arbitrary conducting volume with electrical properties that are independent of any generated potentials. If the volume has no sources on its surface, then the reciprocity theorem states that the potential generated at one location, P_1, from the passage of a unit current at another location, P_2, is equivalent to the potential generated at P_2 from the passage of a unit current at P_1. In other words, there is equivalence between the potential impressed on an electrode from a unit source in neural tissue and the potential generated at the location of the source by an electrode releasing a unit amount of current. It then follows that spatial discriminability of a recording electrode can be studied by analyzing the potentials it generates when acting as a source.

In neural prostheses, such as BMIs, where the goal is to differentiate the electrical activity of individual neurons from nontarget electrical activity in the surrounding tissue, one requires an electrode that—when acting as a source—generates potentials that decay rapidly with distance. The potentials of an arbitrary source decay at a rate $(-\nabla\Phi)$ that is proportional to $\vec{J}$ (Section 4.2.2.1). The geometry that minimizes the surface area of a given unit of volume is a sphere, so the electrode that theoretically

maximizes $-\nabla\Phi$ is a spherical point source whose potentials decay proportional to $1/r$ (Figure 4.6). This explains why electrodes that most resemble a point source, for example, an insulated microelectrode with an exposed sharp tip (Figure 4.1(a) and (c)), are preferred when recording the electrical activity from single units (Robinson, 1968).

In some cases, it is also desirable to have a recording electrode that can measure the aggregate electrical activity of many neurons distributed throughout a volume of tissue. For example, in DBS, simultaneous recording of the electrical activity within the targeted tissue may provide an objective metric for optimizing the selection of stimulation parameters (Kent & Grill, 2011; Priori, Foffani, Rossi, & Marceglia, 2013). These types of recordings require a large (macro) electrode (e.g., Figure 4.1(e)) whose dimensions are on the same order as the length scales being targeted. As the dimensions of an electrode increase, $|\vec{J}|$ decreases, so the potentials of larger electrodes decay much more gradually than $1/r$ (Figure 4.6). Thus, as a general principle, the ability to discriminate spatially larger volumes of tissues increases with electrode size, and the shape of the volume can be tailored by altering the electrode geometry.

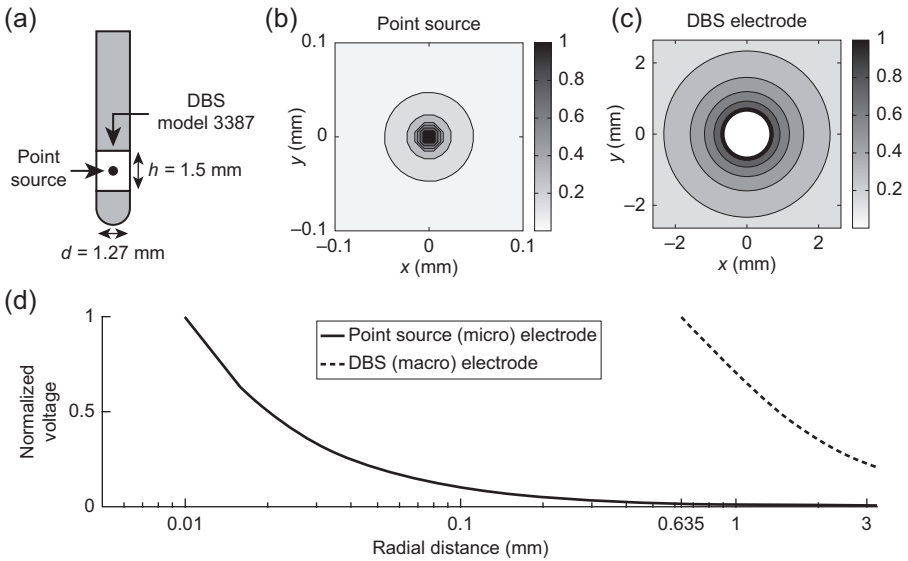

Figure 4.6 Using the reciprocity theorem to assess the effect of electrode geometry on the ability to discriminate spatially different volumes of tissue. (a) A point source and the distal-most contact on the Model 3387 array (Medtronic Inc., Minneapolis, MN) are used to inject separately a unit current into an infinite medium with a homogeneous and isotropic conductivity of 0.2 S/m (Gabriel et al., 2009). (b) Filled contours of the normalized potentials for the point source. (c) The same as (b), except for the 3387 electrode. (d) The potentials impressed on the electrode for a unit current at increasing radial distances from the origin, normalized by the corresponding maximum value. Note: The potentials of the point source were sampled ≥10 μm from the origin.

4.3.1.2 Temporal discrimination

The temporal characteristics of transmembrane currents during the AP vary across different types of electrically excitable cells. APs generated in the axon and soma of neurons have a short duration (approximately 1 ms), so large filter passbands with high cutoffs, typically between 100 and 5–10 kHz, are used to discriminate an ENG, an evoked compound action potential (ECAP), or a single unit (Humphrey & Schmidt, 1991; Rieger et al., 2005; Sacristan & Oses, 2004). However, APs are not the only electrical signals that can be recorded. In neurons, when an AP reaches the axon terminal, neurotransmitter is released and bound to ligand-gated ion channels on the soma and/or dendrites of the postsynaptic neuron. The subsequent flow of ions elicits an electrical event known as a postsynaptic potential (PSP). Compared to an AP, a PSP is longer in duration, lasting anywhere from 1 to 100s of milliseconds, and it can be temporally discriminated from an AP by filtering between 0.5 and 500 Hz (Buzsáki, Anastassiou, & Koch, 2012; Buzsáki & Draguhn, 2004). PSPs and other relatively long lasting signals (e.g., calcium spikes) are predicted to be the origins of LFPs (Buzsáki et al., 2012), so temporal discrimination—regardless of electrode geometry—can be used to differentiate LFPs from single units.

4.3.2 Reduction of electrical noise

A recording electrode should be designed to minimize intrinsic and extrinsic forms of electrical noise, as well as forms of noise that arise from the motion of the electrode and/or tissue.

4.3.2.1 Intrinsic electrical noise

Intrinsic electric noise can be classified into four types: thermal (Johnson or white) noise that arises from the random (Brownian) motion of the charge carriers, flicker (or pink) noise that arises from the changing energy states of the charge carriers, shot noise that arises from the discrete nature of the charge carriers, and generation–recombination (G–R) noise that arises from the statistical generation and recombination of charge carries. All four types of noise have a marked effect at the nanoscale, especially shot noise and G–R noise when recording signals from single ion channels, but at the microscale (single neuron level) and beyond, only the former two have an appreciable effect.

White noise can be reduced by altering the electrical properties of the electrode. Consider a noise source, consisting of a voltage source in series with a noise-generating resistor (R_N), attached to a load (Z_e) that does not generate noise. It can be shown that the root-mean-square voltage across Z_e (V_{white}) obeys the equation

$$V_{\text{white}} = \left(4k_B T R_N \int_0^\infty Z_e\,(f)\; df\right)^{1/2}, \tag{4.8}$$

where k_B is the Boltzmann constant, and T is the absolute temperature of the circuit (Johnson, 1928). We see from Eqn (4.8) that V_{white} can be reduced by reducing the Z_e of the recording electrode.

Z_e can be reduced in three ways (Section 4.2.1.2): by applying a Faradaic electric coating, by roughening the electrode surface, and by increasing the electrode dimensions. All of these approaches can have a marked effect on reducing Z_e, and thereby V_{white}, but with recording electrodes, one should use caution when altering the electrode dimensions. For example, increasing the A of a microelectrode reduces its V_{white} but also reduces the ability to discriminate spatially the electrical activity of single units. Therefore, there is tradeoff between spatial discrimination and noise reduction with microelectrodes, and this is typically minimized by selecting microelectrodes with impedances between 0.1 and 100 MΩ (Robinson, 1968).

Pink noise has an inverse dependence on frequency (f), so unlike white noise, it is not equally present at all frequency ranges (i.e., broadband). Pink noise can be reduced by high pass filtering the recorded signal, but because its effects are independent of Z_e, it is unaffected by electrode design.

4.3.2.2 Extrinsic electrical noise

Electrical noise that originates outside the neural tissue is termed extrinsic noise. External sources of electromagnetic radiation include atmospheric disturbances, such as solar flares and lighting discharges; manmade devices, such as power lines, lighting fixtures, and electrical equipment; and other electrically excitable tissues in the body, such as muscle and cardiac tissue. Although these noise sources are external to the tissue, they can be minimized with certain techniques.

Extrinsic noise can be reduced by subtracting it from the recorded signal using two or more electrodes in a multipolar differential configuration. The simplest example is a bipole. In a bipolar recording, the signal recorded with one electrode (the negative pole) is subtracted from the signal recorded with the second electrode (the positive pole). Noise, of course, can never be completely removed, but it can be attenuated by choosing electrodes that record similar noise waveforms. We know the ability of the electrode to record a signal depends on its geometry (Section 4.3.1.1) and Z_e (Section 4.3.2.1), so contacts on the bipole should have a matching geometry and impedance. Further, as the distance between the electrodes decreases, both the recorded signal and the recorded noise become increasingly similar. Therefore, the bipolar pair should be close enough in proximity that the noise recorded is similar, but not so close that the target signal is also subtracted.

There are instances where use of a multipolar configuration alone is not effective. For example, raw ENG signals are typically on the order of a few microvolts (Rieger et al., 2005), and raw EMG signals are typically on the order of a few millivolts (Reaz, Hussain, & Mohd-Yasin, 2006). Because the nerve and muscle are in close proximity, the SNR is small, and subtraction reduces the neural signal more than the noise. In these instances, insulation and/or electrical shielding can help increase the SNR (Figure 4.7).

In peripheral nerve recordings, insulated tripolar configurations that record $\delta^2\Phi$ between its electrodes are used to attenuate extrinsic noise. The insulation helps by constraining the flow of charge between the electrodes and the nerve. Because sources outside the insulation generate potentials that decay linearly from one end of the constrained space to the other, while the potentials arising from within the nerve do not,

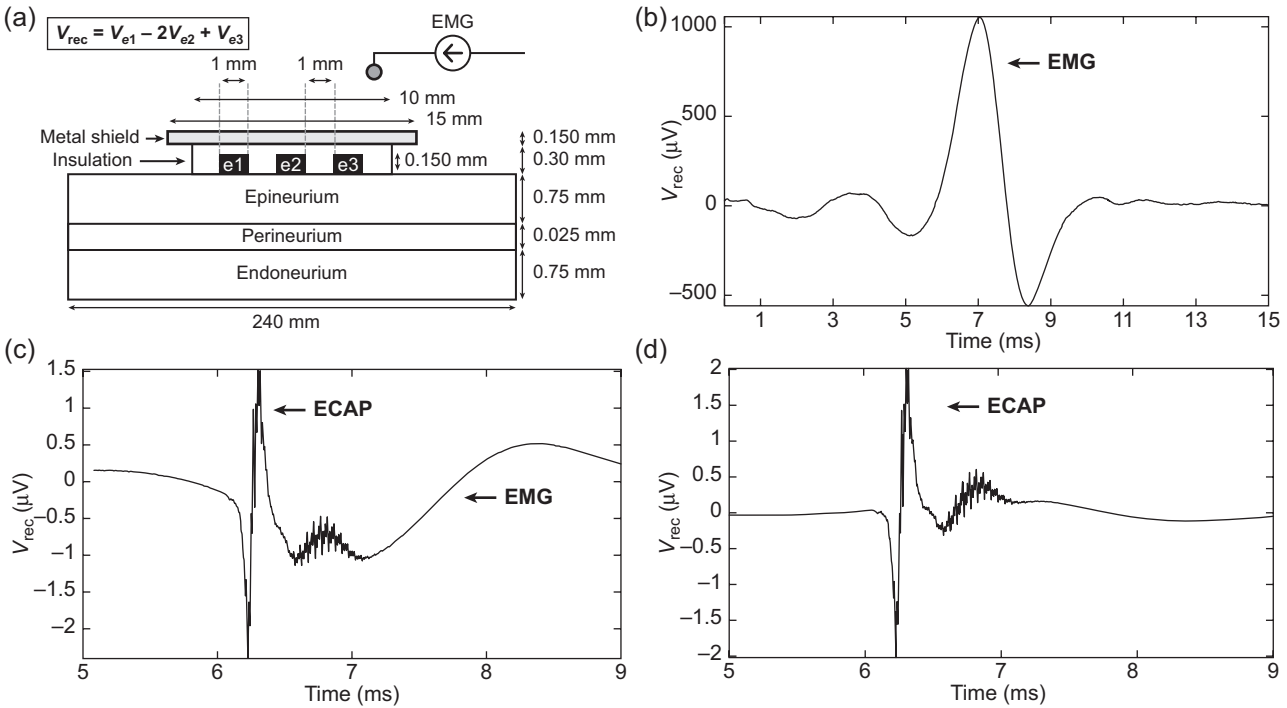

Figure 4.7 Reducing extrinsic noise with a tripolar recording electrode. (a) A population of model axons (Sweeney, Mortimer, & Durand, 1987) is distributed within a nerve, action potentials (APs) are initiated at one end of the nerve, and the resulting ECAP is recorded using a tripolar configuration of three cylindrical electrodes. Extrinsic noise is added by placing a current source that emulates an EMG signal in close proximity to the recording electrodes. Plotted are the recorded responses when the electrodes are (b) neither insulated nor shielded, (c) insulated but not shielded, and (d) both insulated and shielded. The simulations in (a) included 100 axons randomly distributed within an axisymmetric finite-element method model of a nerve. The axons were split into two subpopulations whose diameters were drawn from a normal distribution: 50 axons with $\mu = 2.5\,\mu m$ and $\sigma = 0.3\,\mu m$ and 50 axons with $\mu = 10\,\mu m$ and $\sigma = 1.25\,\mu m$. The model dimensions (not drawn to scale) were representative of the sciatic nerve of a cat (Perez-Orive & Durund, 2000), and the conductivities of the neural tissue were taken from published values (Schiefer, Triolo, & Tyler, 2008).

the tripole works by primarily rejecting extrinsic noise. Of course, toward the edges of the insulation, the potentials beneath the electrodes are no longer linear, so as a general design principle, the distal electrodes should be sufficiently far from the edges (Rahal, Taylor, & Donaldson, 2000; Rahal, Winter, Taylor, & Donaldson, 2000).

In addition to insulation, the SNR can be further increased by electrically shielding the electrodes with a highly conducting metal material—and grounding that material, if possible. Metals are typically 7–8 orders of magnitude less resistive than neural tissue so external currents are diverted around and away from the recording contacts. Although shielding is not currently used in implantable devices, recent work has shown that it can reduce extrinsic noise as much as 80% (Sadeghlo, 2013).

4.3.2.3 Motion artifact

The electrode and surrounding tissue are never truly at rest due to disturbances from physiological processes, such as the cardiac cycle, the respiratory cycle, and muscle contraction. For example, in rats, brain micromotion relative to a stationary implant can be as large as 30 μm during cardiac and respiratory cycles (Gilletti & Muthuswamy, 2006). Movement of the electrode and surrounding tissue relative to each other alters the distribution of charge carriers on either side of the ETI. Since the potential gradient across the ETI (i.e., the half-cell potential) depends on the effective concentrations (activities) of the charge carriers, motion-induced fluctuations in the half-cell potential give rise to another source of extrinsic noise termed *motion artifact*.

Motion artifact can be reduced by stabilizing the charge distribution on either side of the ETI. This cannot be accomplished with polarizable electrodes, such as those made from the noble metals (e.g., Pt, Au, Ir), because their half-cell potentials depend on the distribution of freely moving charge in the surrounding tissue. However, this can be accomplished with nonpolarizable electrodes, where charge is transferred between the electrode and a relatively insoluble layer, because the interface is stable despite movement of the electrode or tissue. One example is the silver/silver chloride (Ag/AgCl) electrode, which is typically used as a surface electrode for recording biopotential signals (Neuman, 2000). Ag/AgCl surface electrodes not only mitigate motion artifact from skin movement with respect to the electrode, they can also be recessed and filled with a conductive fluid/gel to further mitigate movement of charge at the ETI (Neuman, 2000). Ag/AgCl is toxic within the body (Geddes & Roeder, 2003), so biocompatible materials, such as PtIr, that have both polarizable and nonpolarizable behavior are recommended to reduce motion artifact in implanted electrodes.

In cases where the electronic noise and signal occupy two separate bandwidths, noise can be further reduced through the use of electronic filtering. For example, motion artifacts typically occupy a bandwidth of <5 Hz, so motion artifacts can be reduced by filtering, independent of the electrode geometry and configuration, and still preserve most or all of the energy in the target signal.

4.3.3 Designing nondamaging recording electrodes

The input impedance of the recording instrumentation (i.e., electrode + amplifier) is typically many orders of magnitude larger than the lumped impedance of the tissue. As

a result, recording electrodes operate under very low current density conditions, and irreversible electrochemical reactions that degrade the electrode and/or damage tissue do not occur. Yet, implantation and presence of the electrode elicit a passive tissue response that may degrade the performance of the electrode, so whether for recording or stimulation purposes, implanted electrodes must mitigate the passive tissue response.

4.3.3.1 The passive tissue response

Neural tissue is displaced during implantation, severing capillaries, extracellular matrix (ECM), and glial and neuronal processes. As blood-borne cells and proteins enter the tissue, the wound healing process is initiated. Hemostasis occurs within the first seconds to hours, where the formation of a clot prevents further bleeding and spread of pathogens, and molecules within the clot signal the start of the inflammation process (Stroncek & Reichert, 2007). Within the next hours to days, the inflammation process clears the cellular debris, contains and neutralizes the injury-causing agent (i.e., the electrode), and mitigates further damage to the tissue (Anderson, 2001). In the CNS, this is mediated by microglia and astrocytes, and in the PNS and muscle, this is mediated by leukocytes and macrophages (Stroncek & Reichert, 2007). After several days, the inflammation process subsides and transitions into a process of repair that lasts for days to weeks.

Axons and tissue in the PNS can regenerate to a significant degree, as long as the soma of the axon remains viable and the perineurium and epineurium remain intact (Sunderland, 1991). In more severe cases, where disruption of the endoneurium and/or perineurium results in the rupturing of the blood–nerve barrier, extensive fibrous ECM (i.e., fibrosis) is required to repair the damaged tissue (Sunderland, 1991). Neurons and tissue in the CNS, however, do not regenerate. Astrocytes, recruited in a process known as gliosis, form a boundary (or glial scar) around the damaged tissue. The glial scar limits the spread of inflammatory cells and aids in the repair of the blood–brain barrier (Norenberg, 2005; Silver & Miller, 2004), but it also inhibits the growth of new axons and signals the degradation of ECM (Stroncek & Reichert, 2007). For up to several months, the glial scar encapsulating the electrode increases in density (Turner et al., 1999), and a similar response is expected for fibrous scar tissue in the PNS (Grill & Mortimer, 2000).

Scarring both helps and hinders the performance of a recording electrode. Scar tissue has a ρ of 5–20 Ω-m (Grill & Mortimer, 1994), whereas brain tissue has a ρ of 3.3–5 Ω-m (Butson, Maks, & Mcintyre, 2006). Indeed, a greater ρ leads to a greater voltage drop across the scar tissue—as $\vec{J} \cdot \rho = -\nabla \Phi$—but because the electrode is encapsulated by the tissue, a distributed voltage divider is created that helps by increasing the amplitude of the recorded signal (Lowery, Weir, & Kuiken, 2006; Moffitt & McIntyre, 2005). Scar tissue, however, also limits the proximity of the electrode and target elements. For example, the glial scar surrounding a microelectrode typically has a thickness of 5–75 μm, although it can be as thick as 250 μm (Edell, Toi, Mcneil, & Clark, 1992). Because recording signals from a single neuron require that the electrode lie within ~100–200 μm of the active neuron (Figure 4.6(d)), the adverse effect of scarring on the recorded signal can be greater than its helpful effect (Figure 4.8).

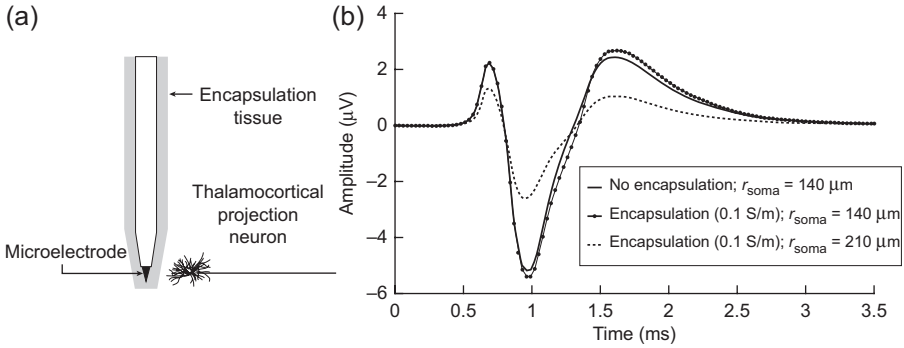

Figure 4.8 The effect of the passive tissue response on microelectrode recordings of single units. (a) An insulated microelectrode with an exposed sharp tip (area ~324 μm^2) is placed in gray matter and used to record the electrical activity of a thalamacortical projection neuron (Mcintyre, Grill, Sherman, & Thakor, 2004). (b) Single unit recordings taken when no encapsulation tissue is present and the (soma of the) neuron is 140 μm from the electrode surface, when 50-μm-thick encapsulation tissue is present and the neuron is 140 μm from the electrode, and when 100 μm thick encapsulation tissue is present and the neuron is 210 μm from the electrode. For the simulation in (a), the gray matter had a conductivity of 0.2 S/m (Gabriel et al., 2009), and the encapsulation tissue had a conductivity of 0.1 S/m (Butson et al., 2006). The recorded potentials were calculated by numerically solving a single reciprocal problem with the finite-element method (Moffitt & Mcintyre, 2005).

The electrical effects of scarring on the surrounding tissue stabilize after several weeks (Ludwig, Uram, Yang, Martin, & Kipke, 2006). In instances where the scarring is minimal, the signal amplitude declines, but not enough to substantially degrade the recording performance (Merrill & Tresco, 2005). Yet, recording failures still occur. In these instances, recording failures are better explained by a local neurodegenerative state surrounding the electrode—characterized by neuron loss, dendrite loss, and axon pathology—that is believed to result from chronic inflammation (Mcconnell et al., 2009). Thus, the chronic inflammatory response can also be deleterious to the performance of the recording electrode.

4.3.3.2 Mitigating the passive tissue response

In the CNS, the overall magnitude of glial activation is dependent on the extent of damage to the blood–brain barrier and tissue (Silver & Miller, 2004). Certainly, the blood–brain barrier and tissue incur damage during implantation, but damage also results from the residence of the electrode within the tissue, as movement of the electrode and tissue causes tissue compression and tearing (He & Bellamkonda, 2007). The same is also expected to be true in the PNS (Grill & Mortimer, 2000; Lefurge, Goodall, Horch, Stensaas, & Schoenberg, 1991). Therefore, damage incurred acutely during implantation should be distinguished from chronic damage incurred while the electrode resides in the tissue.

The acute response of the tissue to implantation depends on the geometry and surface texture of the electrode (Edell et al., 1992; Szarowski et al., 2003). Electrodes

with larger cross-sectional areas and rough textures (i.e., sharp edges) have a more severe initial response than smaller electrodes with smooth surfaces (Szarowski et al., 2003), so the acute response of the tissue can be mitigated by using smaller electrodes with smoother surfaces. This is only advantageous, however, as long as altering the geometry and surface texture of the electrode does not degrade its performance. Recall, reducing the size of a recording electrode increases the amplitude of white noise (Section 4.3.2.1), while at the same time decreasing its ability to record activity from large volumes of tissue (Section 4.3.1.1); and reducing the size of a stimulation electrode increases Z_e, which decreases its efficiency (Section 4.2.1.2).

Unlike the acute response, the chronic response of the tissue to the presence of the electrode is independent of its geometry and surface texture (Edell et al., 1992; Szarowski et al., 2003). One apparent influence on the chronic tissue response is the large disparity between the mechanical properties of the rigid electrode substrate, typically silicon, and the soft neural tissue. For example, silicon has an elastic modulus of ~200 GPa (Pearson, Read, & Feldmann, 1957), while brain tissue has an elastic modulus of 6 kPa (Ommaya, 1968). Therefore, when the electrode or tissue moves (e.g., during brain micromotion), the large mismatch in stiffness has the potential to generate mechanical forces that deform and tear the tissue (He & Bellamkonda, 2007).

The mismatch in stiffness between the electrode and tissue can be reduced by applying a conductive polymer coating to the electrode surface. Two widely used conductive polymers are polypyrrole (PPy) and poly(3,4-ethylenedioxythiophene) (PEDOT) because of their many advantages in addition to reducing mechanical stress. PPy and PEDOT are stable, biocompatible (Cui & Martin, 2003; George et al., 2005), and support the growth of neurons and neurites (Yang et al., 2005). In addition, these polymers can also be used to decrease Z_e by roughening the electrode surface. PEDOT, for example, has been used to decrease the Z_e of gold microelectrodes by one to two orders of magnitude (Ludwig et al., 2011). Because surface roughening does not affect the macroscopic dimensions of the electrode, conductive polymer coatings reduce mechanical stress on the tissue, while at the same time improving the SNR by reducing V_{white} (Ludwig et al., 2011, 2006).

Another origin of the chronic tissue response is persistent inflammation. Microglia, macrophages, and other inflammatory cells clear foreign and necrotic debris at the site of implantation. The electrode, also viewed as a foreign body, is nondegradable and too large to undergo phagocytosis, so the macrophages form giant multinucleated cells that continuously release degradative agents, such as superoxides and free radicals, into the tissue (He & Bellamkonda, 2007; Polikov et al., 2005). This process, known as “frustrated phagocytosis”, damages both the foreign body and the surrounding tissue, and is an additional potential explanation for why neurons and dendrites are lost, despite stabilization of the glial scar (McConnell et al., 2009).

There are passive and active strategies for reducing the inflammatory response. Passive strategies attempt to reduce inflammation by preventing the adsorption of nonspecific proteins and inflammatory cells on the electrode surface. Examples of this include pretreating the electrode with cells or proteins, such as albumin, that elicit little to no inflammatory response, or by coating the electrode with polymers, such as polyethylene glycol, that resist protein adsorption (Bridges & García, 2008). Passive

strategies are straightforward and simple, but their performance in vivo is still inconclusive (Bridges & García, 2008). Active strategies, in contrast, attempt to reduce inflammation by using the electrode to deliver anti-inflammatory agents, including dexamethasone, heparin, and alpha melanocyte-stimulating hormone. Agents can be delivered via diffusion from polymer coatings and hydrogels, such as PPy (Wadhwa, Lagenaur, & Cui, 2006) and sodium alginate (Kim, Abidian, & Martin, 2004), respectively, or via dissolution from biodegradable coatings, such as polylactic acid (PLA) (Anderson & Shive, 2012). These strategies, although more complex, offer fine control over the presentation and kinetics of immunomodulatory agents.

4.4 Future directions

Creating stimulation electrodes that are efficient, selective, and nondamaging requires the development of new technologies. Vertically aligned carbon nanofiber (CNF) arrays are of one the emerging technologies that show great promise in increasing stimulation efficiency by reducing Z_e. CNF arrays form a highly porous surface area that is freely accessible to charge. Unmodified, CNF arrays have a c_{dl} of ~0.4 mF/cm^2, which is greater than the c_{dl} of conventional noble metal electrodes (~20 μF/cm^2) (Wei & Grill, 2009), but less than the c_{dl} of PtIr electrodes (~0.6 mF/cm^2) used in therapies, such as DBS and SCS (Nguyen-Vu et al., 2006). However, when modified with a coating of PPy, CNF arrays have an effective c_{dl} (i.e., including pseudo-capacitance) that can be as large as 100 mF/cm^2 (Nguyen-Vu et al., 2006), and as a result, they have the potential of being more efficient than PtIr electrodes (de Asis et al., 2009). The in vivo biocompatibility of CNF arrays is still inconclusive, so their future success depends on continuing research (Asis, Andrews, & Li, 2012; Nguyen-Vu et al., 2006; Smart, Cassady, Lu, & Martin, 2006).

As fabrication techniques improve, high density arrays (HDAs) consisting of hundreds to thousands of electrodes will emerge. HDAs show great promise in increasing stimulation selectivity: electrodes can be used separately to target small volumes of tissue (Martens et al., 2011) or combined to form macroelectrode geometries, or electrodes can be combined in multipolar configurations to shape the generated fields (Keane et al., 2012). Yet, implementation of HDAs will have some issues. As electrodes decrease in size, greater power densities and charge densities will lead to increased heat generation and the propensity for tissue damage, respectively (Shannon, 1992); and as the number of electrodes increases so will the difficulty in programming the device.

Emerging technologies also hold great promise for creating more effective recording electrodes. There have been considerable advancements over the past decades in increasing the discriminability and noise rejection capabilities of recording electrodes, but many challenges still remain for minimizing the tissue response. The biggest of these challenges is reducing the chronic inflammatory response, as it has a marked impact on neuron viability (Kim et al., 2004; McConnell et al., 2009) and thereby the long-term stability of the recordings (Lebedev & Nicolelis, 2006). The majority of emerging technologies focus on reducing neuron losses by eliminating inflammation,

but neuron losses can also be reduced by promoting their growth and survival using neurotrophic factors. Designs that employ this strategy are known as neurotrophic electrodes, which have been studied for over two decades.

The most studied neurotrophic electrode is the cone electrode, consisting of a conical hollow glass tube containing metal wires and a neurotrophic medium that promotes the growth of dendrites and axons (Kennedy, 1989; Kennedy, Mirra, & Bakay, 1992). Such a design is advantageous because it brings neurites in close proximity to the electrode, while at the same time isolating the neurite from potentially harmful inflammatory factors. Neurotrophic electrodes have had much success, particularly in humans, where they have been able to isolate single units for over 4 years (Kennedy, 2012). However, despite remarkable stability, neurotrophic electrodes are not widely used because their relatively large size (of hundreds of microns) limits their ability to isolate multiple neurons in close proximity. As technology progresses, miniaturization of the substrate and wires will allow for multiple isolated cavities to be used to spatially discriminate many signals at once.

Acknowledgments

Preparation of this chapter was supported by the National Institute of Health under Grant R01 NS040894 and a Ruth L. Kirschstein Predoctoral Fellowship, F31 NS079105.

References

Alo, K. M., Yland, M. J., Kramer, D. L., Charnov, J. H., & Redko, V. (1998). Computer assisted and patient interactive programming of dual octrode spinal cord stimulation in the treatment of chronic pain. *Neuromodulation*, *1*, 30.

Anderson, J. M. (2001). Biological responses to materials. *Annual Review of Materials Research*, *31*, 81–110.

Anderson, J. M., & Shive, M. S. (2012). Biodegradation and biocompatibility of PLA and PLGA microspheres. *Advanced Drug Delivery Reviews*, *64*, 72–82 Supplement.

Asis, E. D., Andrews, R. J., & Li, J. (2012). *Nanomedicine and the nervous system*. New York: CRC Press.

de Asis, E., Jr, Nguyen-Vu, T. D. B., Arumugam, P., Chen, H., Cassell, A., Andrews, R., et al. (2009). High efficient electrical stimulation of hippocampal slices with vertically aligned carbon nanofiber microbrush array. *Biomedical Microdevices*, *11*, 801–808.

Bell, G. K., Kidd, D., & North, R. B. (1997). Cost-effectiveness analysis of spinal cord stimulation in treatment of failed back surgery syndrome. *Journal of Pain and Symptom Management*, *13*, 286–295.

Birdno, M. J., Kuncel, A. M., Dorval, A. D., Turner, D. A., Gross, R. E., & Grill, W. M. (2012). Stimulus features underlying reduced tremor suppression with temporally patterned deep brain stimulation. *Journal of Neurophysiology*, *107*, 364–383.

Boviatsis, E. J., Stavrinou, L. C., Themistocleous, M., Kouyialis, A. T., & Sakas, D. E. (2010). Surgical and hardware complications of deep brain stimulation. A seven-year experience and review of the literature. *Acta Neurochirurgica (Wien)*, *152*, 2053–2062.

Branner, A., & Normann, R. A. (2000). A multielectrode array for intrafascicular recording and stimulation in sciatic nerve of cats. *Brain Research Bulletin*, *51*, 293–306.

Bridges, A. W., & García, A. J. (2008). Biocompatibility of implanted diabetes devices: Part 2: Anti-inflammatory polymeric coatings for implantable biomaterials and devices. *Journal of Diabetes Science and Technology*, *2*, 984 (Online).

Bronstein, J. M., Tagliati, M., Alterman, R. L., Lozano, A. M., Volkmann, J., Stefani, A., et al. (2011). Deep brain stimulation for parkinson disease: an expert consensus and review of key issues. *Archives of Neurology*, *68*, 165.

Budai, D. (2010). *Carbon fiber-based microelectrodes and microbiosensors*.

Butson, C. R., Maks, C. B., & Mcintyre, C. C. (2006). Sources and effects of electrode impedance during deep brain stimulation. *Clinical Neurophysiology*, *117*, 447–454.

Buzsáki, G., Anastassiou, C. A., & Koch, C. (2012). The origin of extracellular fields and currents — EEG, ECoG, LFP and spikes. *Nature Reviews Neuroscience*, *13*, 407–420.

Buzsáki, G., & Draguhn, A. (2004). Neuronal oscillations in cortical networks. *Science*, *304*, 1926–1929.

Cameron, T. (2004). Safety and efficacy of spinal cord stimulation for the treatment of chronic pain: a 20-year literature review. *Journal of Neurosurgery: Spine*, *100*, 254–267.

Chaudhury, D., Walsh, J. J., Friedman, A. K., Juarez, B., Ku, S. M., Koo, J. W., et al. (2012). Rapid regulation of depression-related behaviours by control of midbrain dopamine neurons. *Nature* advance online publication.

Cicione, R., Shivdasani, M. N., Fallon, J. B., Luu, C. D., Allen, P. J., Rathbone, G. D., et al. (2012). Visual cortex responses to suprachoroidal electrical stimulation of the retina: effects of electrode return configuration. *Journal of Neural Engineering*, *9*, 036009.

Coffey, R. J. (2001). Deep brain stimulation for chronic pain: results of two multicenter trials and a structured review. *Pain Medicine*, *2*, 183–192.

Cogan, S. F. (2008). Neural stimulation and recording electrodes. *Annual Review of Biomedical Engineering*, *10*, 275–309.

Cui, X., & Martin, D. C. (2003). Electrochemical deposition and characterization of poly(3,4-ethylenedioxythiophene) on neural microelectrode arrays. *Sensors and Actuators B: Chemical*, *89*, 92–102.

Edell, D. J., Toi, V. V., Mcneil, V. M., & Clark, L. D. (1992). Factors influencing the biocompatibility of insertable silicon microshafts in cerebral cortex. *Biomedical Engineering, IEEE Transactions on*, *39*, 635–643.

Elger, C. E., & Lehnertz, K. (1998). Seizure prediction by non-linear time series analysis of brain electrical activity. *European Journal of Neuroscience*, *10*, 786–789.

Ellis, T. M., Foote, K. D., Fernandez, H. H., Sudhyadhom, A., Rodriguez, R. L., Zeilman, P., et al. (2008). Reoperation for suboptimal outcomes after deep brain stimulation surgery. *Neurosurgery*, *63*, 754–760 discussion 760–1.

Elwassif, M. M., Datta, A., Rahman, A., & Bikson, M. (2012). Temperature control at DBS electrodes using a heat sink: experimentally validated FEM model of DBS lead architecture. *Journal of Neural Engineering*, *9*, 046009.

Elwassif, M. M., Kong, Q., Vazquez, M., & Bikson, M. (2006). Bio-heat transfer model of deep brain stimulation-induced temperature changes. *Journal of Neural Engineering*, *3*, 306.

Fang, Z. P., & Mortimer, J. T. (1991a). A method to effect physiological recruitment order in electrically activated muscle. *IEEE Transactions on Biomedical Engineering*, *38*, 175–179.

Fang, Z. P., & Mortimer, J. T. (1991b). Selective activation of small motor axons by quasitrapezoidal current pulses. *IEEE Transactions on Biomedical Engineering*, *38*, 168–174.

Foldes, E. L., Ackermann, D. M., Bhadra, N., Kilgore, K. L., & Bhadra, N. (2011). Design, fabrication and evaluation of a conforming circumpolar peripheral nerve cuff electrode for acute experimental use. *Journal of Neuroscience Methods*, *196*, 31–37.

Gabriel, C., Peyman, A., & Grant, E. H. (2009). Electrical conductivity of tissue at frequencies below 1 MHz. *Physics in Medicine and Biology*, *54*, 4863–4878.

Geddes, L. A., & Roeder, R. (2003). Criteria for the selection of materials for implanted electrodes. *Annals of Biomedical Engineering*, *31*, 879–890.

George, P. M., Lyckman, A. W., Lavan, D. A., Hegde, A., Leung, Y., Avasare, R., et al. (2005). Fabrication and biocompatibility of polypyrrole implants suitable for neural prosthetics. *Biomaterials*, *26*, 3511–3519.

Gilletti, A., & Muthuswamy, J. (2006). Brain micromotion around implants in the rodent somatosensory cortex. *Journal of Neural Engineering*, *3*, 189.

Goldstein, L. S., Dewhirst, M. W., Repacholi, M., & Kheifets, L. (2003). Summary, conclusions and recommendations: adverse temperature levels in the human body. *International Journal of Hyperthermia*, *19*, 373–384.

Gosalia, K., Weiland, J., Humayun, M., & Lazzi, G. (2004). Thermal elevation in the human eye and head due to the operation of a retinal prosthesis. *IEEE Transactions on Biomedical Engineering*, *51*, 1469–1477.

Gradinaru, V., Mogri, M., Thompson, K. R., Henderson, J. M., & Deisseroth, K. (2009). Optical deconstruction of parkinsonian neural circuitry. *Science*, *324*, 354–359.

Grill, W. M., & Mortimer, J. T. (1994). Electrical properties of implant encapsulation tissue. *Annals of Biomedical Engineering*, *22*, 23–33.

Grill, W. M., & Mortimer, J. T. (2000). Neural and connective tissue response to long-term implantation of multiple contact nerve cuff electrodes. *Journal of Biomedical Materials Research*, *50*, 215–226.

He, W., & Bellamkonda, R. V. (2007). A molecular perspective on understanding and modulating the performance of chronic central nervous sytem (CNS) recording electrodes. In W. M. Reichert (Ed.), *Indwelling neural implants: Strategies for contending with the in vivo environment*. Boca Raton: CRC Press.

Hodaie, M., Wennberg, R. A., Dostrovsky, J. O., & Lozano, A. M. (2002). Chronic anterior thalamus stimulation for intractable epilepsy. *Epilepsia*, *43*, 603–608.

Holsheimer, J. (1998). Computer modelling of spinal cord stimulation and its contribution to therapeutic efficacy. *Spinal Cord*, *36*, 531–540.

Holsheimer, J. (2002). Which neuronal elements are activated directly by spinal cord stimulation. *Neuromodulation*, *5*, 25–31.

Holsheimer, J., Struijk, J. J., & Wesselink, W. A. (1998). Analysis of spinal cord stimulation and design of epidural electrodes by computer modeling. *Neuromodulation: Technology at the Neural Interface*, *1*, 14–18.

Howell, B., & Grill, W. M. (2014). Evaluation of high-perimeter electrode designs for deep brain stimulation. *Journal of Neural Engineering*, *11*, 1741–2560.

Humphrey, D., & Schmidt, E. (1991). Extracellular single-unit recording methods. In A. Boulton, G. Baker, & C. Vanderwolf (Eds.), *Neurophysiological techniques*. Humana Press.

Jezernik, S., Craggs, M., Grill, W. M., Creasey, G., & Rijkhoff, N. J. M. (2002). Electrical stimulation for the treatment of bladder dysfunction: current status and future possibilities. *Neurological Research*, *24*, 413–430.

Johnson, J. B. (1928). Thermal agitation of electricity in conductors. *Physical Review*, *32*, 97–109.

Keane, M., Deyo, S., Abosch, A., Bajwa, J. A., & Johnson, M. D. (2012). Improved spatial targeting with directionally segmented deep brain stimulation leads for treating essential tremor. *Journal of Neural Engineering*, *9*, 046005.

Kennedy, P. R. (1989). The cone electrode: a long-term electrode that records from neurites grown onto its recording surface. *Journal of Neuroscience Methods*, *29*, 181–193.

Kennedy, P. (2012). Reliable neural interface: the first quarter century of the neurotrophic electrode. In *Engineering in medicine and biology society (EMBC), 2012 annual international conference of the IEEE* (pp. 3332–3335). IEEE.

Kennedy, P. R., Mirra, S. S., & Bakay, R. a. E. (1992). The cone electrode: ultrastructural studies following long-term recording in rat and monkey cortex. *Neuroscience Letters*, *142*, 89–94.

Kent, R. A., & Grill, M. W. (2013). Model-based analysis and design of nerve cuff electrodes for restoring bladder function by selective stimulation of the pudendal nerve. *Journal of Neural Engineering*, *10*, 036010.

Kent, A. R., & Grill, W. M. (2011). Instrumentation to record evoked potentials for closed-loop control of deep brain stimulation. In *Engineering in medicine and biology society, EMBC, 2011 annual international conference of the IEEE* (pp. 6777–6780). IEEE.

Kim, D.-H., Abidian, M., & Martin, D. C. (2004). Conducting polymers grown in hydrogel scaffolds coated on neural prosthetic devices. *Journal of Biomedical Materials Research Part A*, *71A*, 577–585.

Kleiner-Fisman, G., Herzog, J., Fisman, D. N., Tamma, F., Lyons, K. E., Pahwa, R., et al. (2006). Subthalamic nucleus deep brain stimulation: summary and meta-analysis of outcomes. *Movement Disorders*, *21*, S290–S304.

Kuhn, J., Grundler, T. O., Lenartz, D., Sturm, V., Klosterkotter, J., & Huff, W. (2010). Deep brain stimulation for psychiatric disorders. *Deutsches Aerzteblatt International*, *107*, 105–113.

Kuncel, A. M., & Grill, W. M. (2004). Selection of stimulus parameters for deep brain stimulation. *Clinical Neurophysiology*, *115*, 2431–2441.

Lebedev, M. A., & Nicolelis, M. a. L. (2006). Brain–machine interfaces: past, present and future. *Trends in Neurosciences*, *29*, 536–546.

Lefurge, T., Goodall, E., Horch, K., Stensaas, L., & Schoenberg, A. (1991). Chronically implanted intrafascicular recording electrodes. *Annals of Biomedical Engineering*, *19*, 197–207.

Lertmanorat, Z., & Durand, M. D. (2004). Extracellular voltage profile for reversing the recruitment order of peripheral nerve stimulation: a simulation study. *Journal of Neural Engineering*, *1*, 202.

Lertmanorat, Z., Gustafson, K., & Durand, D. (2006). Electrode array for reversing the recruitment order of peripheral nerve stimulation: experimental studies. *Annals of Biomedical Engineering*, *34*, 152–160.

Limousin, P., Speelman, J. D., Gielen, F., & Janssens, M. (1999). Multicentre European study of thalamic stimulation in parkinsonian and essential tremor. *Journal of Neurology, Neurosurgery & Psychiatry*, *66*, 289–296.

Lowery, M. M., Weir, R. F., & Kuiken, T. A. (2006). Simulation of intramuscular EMG signals detected using implantable myoelectric sensors (IMES). *IEEE Transactions on Biomedical Engineering*, *53*, 1926–1933.

Ludwig, K. A., Langhals, N. B., Joseph, M. D., Richardson-Burns, S. M., Hendricks, J. L., & Kipke, D. R. (2011). Poly(3,4-ethylenedioxythiophene) (PEDOT) polymer coatings facilitate smaller neural recording electrodes. *Journal of Neural Engineering*, *8*, 014001.

Ludwig, K. A., Uram, J. D., Yang, J., Martin, D. C., & Kipke, D. R. (2006). Chronic neural recordings using silicon microelectrode arrays electrochemically deposited with a poly(3,4-ethylenedioxythiophene) (PEDOT) film. *Journal of Neural Engineering*, *3*, 59.

Manola, L., & Holsheimer, J. (2004). Technical performance of percutaneous and laminectomy leads analyzed by modeling. *Neuromodulation: Technology at the Neural Interface*, *7*, 231–241.

Martens, H. C. F., Toader, E., Decré, M. M. J., Anderson, D. J., Vetter, R., Kipke, D. R., et al. (2011). Spatial steering of deep brain stimulation volumes using a novel lead design. *Clinical Neurophysiology*, *122*, 558–566.

Mayberg, H. S., Lozano, A. M., Voon, V., Mcneely, H. E., Seminowicz, D., Hamani, C., et al. (2005). Deep brain stimulation for treatment-resistant depression. *Neuron*, *45*, 651–660.

McConnell, G. C., Rees, H. D., Levey, A. I., Gutekunst, C. A., Gross, R. E., & Bellamkonda, R. V. (2009). Implanted neural electrodes cause chronic, local inflammation that is correlated with local neurodegeneration. *Journal of Neural Engineering*, *6*, 056003.

Mccreery, D. B., Agnew, W. F., Yuen, T. G. H., & Bullara, L. (1990). Charge density and charge per phase as cofactors in neural injury induced by electrical stimulation. *IEEE Transactions on Biomedical Engineering*, *37*, 996–1001.

Mcintyre, C., & Grill, W. (2000). Selective microstimulation of central nervous system neurons. *Annals of Biomedical Engineering*, *28*, 219–233.

Mcintyre, C. C., Grill, W. M., Sherman, D. L., & Thakor, N. V. (2004). Cellular effects of deep brain stimulation: model-based analysis of activation and inhibition. *Journal of Neurophysiology*, *91*, 1457–1469.

Merrill, D. R., Bikson, M., & Jefferys, J. G. (2005). Electrical stimulation of excitable tissue: design of efficacious and safe protocols. *Journal of Neuroscience Methods*, *141*, 171–198.

Merrill, D. R., & Tresco, P. A. (2005). Impedance characterization of microarray recording electrodes in vitro. *IEEE Transactions on Biomedical Engineering*, *52*, 1960–1965.

Moffitt, M. A., & McIntyre, C. C. (2005). Model-based analysis of cortical recording with silicon microelectrodes. *Clinical Neurophysiology*, *116*, 2240–2250.

Montgomery, E. B., Jr. (1999). Deep brain stimulation reduces symptoms of Parkinson disease. *Cleveland Clinic Journal of Medicine*, *66*, 9–11.

Murray, J. A., & Blakemore, W. F. (1980). The relationship between internodal length and fibre diameter in the spinal cord of the cat. *Journal of the Neurological Sciences*, *45*, 29–41.

Neuman, M. R. (2000). Biopotential electrodes. In D. J. Bronzino (Ed.), *The biomedical engineering handbook*. Boca Raton: CRC Press.

Nguyen-Vu, T. D. B., Chen, H., Cassell, A. M., Andrews, R., Meyyappan, M., & Li, J. (2006). Vertically aligned carbon nanofiber arrays: an advance toward electrical–neural interfaces. *Small*, *2*, 89–94.

Norenberg, M. (2005). The reactive astrocyte. *The Role of Glia in Neurotoxicity*, *2*, 73–93.

Norlin, A., Pan, J., & Leygraf, C. (2002). Investigation of interfacial capacitance of Pt, Ti and TiN coated electrodes by electrochemical impedance spectroscopy. *Biomolecular Engineering*, *19*, 67–71.

Okun, M. S., Rodriguez, R. L., Foote, K. D., Sudhyadhom, A., Bova, F., Jacobson, C., et al. (2008). A case-based review of troubleshooting deep brain stimulator issues in movement and neuropsychiatric disorders. *Parkinsonism & Related Disorders*, *14*, 532–538.

Okun, M. S., Tagliati, M., Pourfar, M., Fernandez, H. H., Rodriguez, R. L., Alterman, R. L., et al. (2005). Management of referred deep brain stimulation failures: a retrospective analysis from 2 movement disorders centers. *Archives of Neurology*, *62*, 1250–1255.

Ommaya, A. K. (1968). Mechanical properties of tissues of the nervous system. *Journal of Biomechanics*, *1*, 127–138.

Pearson, G. L., Read, W. T., Jr, & Feldmann, W. L. (1957). Deformation and fracture of small silicon crystals. *Acta Metallurgica*, *5*, 181–191.

Peckham, P. H., & Knutson, J. S. (2005). Functional electrical stimulation for neuromuscular applications. *Annual Review of Biomedical Engineering*, *7*, 327–360.

Pendekanti, R., & Henriquez, C. S. (1996). Spatial potential and current distributions along transvenous defibrillation electrodes: variation of electrode characteristics. *Annals of Biomedical Engineering*, *24*, 156–167.

Pennes, H. H. (1948). Analysis of tissue and arterial blood temperatures in the resting human forearm. *Journal of Applied Physiology*, *1*, 93–122.

Perez-Orive, J., & Durund, D. M. (2000). Modeling study of peripheral nerve recording selectivity. *IEEE Transactions on Rehabilitation Engineering*, *8*, 320–329.

Plonsey, R. (1963). Reciprocity applied to volume conductors and the ECG. *IEEE Transactions on Bio-medical Electronics*, *10*, 9–12.

Polikov, V. S., Tresco, P. A., & Reichert, W. M. (2005). Response of brain tissue to chronically implanted neural electrodes. *Journal of Neuroscience Methods*, *148*, 1–18.

Priori, A., Foffani, G., Rossi, L., & Marceglia, S. (2013). Adaptive deep brain stimulation (aDBS) controlled by local field potential oscillations. *Experimental Neurology*, *245*, 77–86.

Rahal, M., Taylor, J., & Donaldson, N. (2000). The effect of nerve cuff geometry on interference reduction: a study by computer modeling. *IEEE Transactions on Biomedical Engineering*, *47*, 136–138.

Rahal, M., Winter, J., Taylor, J., & Donaldson, N. (2000). An improved configuration for the reduction of EMG in electrode cuff recordings: a theoretical approach. *IEEE Transactions on Biomedical Engineering*, *47*, 1281–1284.

Rattay, F. (1986). Analysis of models for external stimulation of axons. *IEEE Transactions on Biomedical Engineering, BME*, *33*, 974–977.

Rattay, F., & Resatz, S. (2004). Effective electrode configuration for selective stimulation with inner eye prostheses. *IEEE Transactions on Biomedical Engineering*, *51*, 1659–1664.

Reaz, M. B. I., Hussain, M. S., & Mohd-Yasin, F. (2006). Techniques of EMG signal analysis: detection, processing, classification and applications. *Biological Procedures Online*, *8*, 11–35.

Rieger, R., Pal, D., Taylor, J., Clarke, C., Langlois, P., Donaldson, N., et al. (2005). 10-channel very low noise ENG amplifier system using CMOS technology. In *IEEE international symposium on circuits and systems, 2005. ISCAS 2005. 23–26 May 2005* (Vol. 1) (pp. 748–751).

Rizzo, J. F., & Wyatt, J. (1997). REVIEW: Prospects for a visual prosthesis. *The Neuroscientist*, *3*, 251–262.

Robinson, D. A. (1968). The electrical properties of metal microelectrodes. *Proceedings of the IEEE*, *56*, 1065–1071.

Rose, T. L., Kelliher, E. M., & Robblee, L. S. (1985). Assessment of capacitor electrodes for intracortical neural stimulation. *Journal of Neuroscience Methods*, *12*, 181–193.

Sackeim, H. A., Rush, A. J., George, M. S., Marangell, L. B., Husain, M. M., Nahas, Z., et al. (2001). Vagus nerve stimulation (VNS[trade]) for treatment-resistant depression: efficacy, side effects, and predictors of outcome. *Neuropsychopharmacology*, *25*, 713–728.

Sacristan, J., & Oses, M. T. (2004). Low noise amplifier for recording ENG signals in implantable systems. In *Proceedings of the 2004 international symposium on circuits and systems, 2004. ISCAS '04. 23–26 May 2004* (Vol. 4) (pp. IV-33–36).

Sadeghlo, B. (2013). *Design of a peripheral nerve electrode for improved neural recording of the cervical vagus nerve*. Masters of Applied Science. University of Toronto.

Schachter, S. C., & Saper, C. B. (1998). Vagus nerve stimulation. *Epilepsia*, *39*, 677–686.

Schiefer, M. A., & Grill, W. M. (2006). Sites of neuronal excitation by epiretinal electrical stimulation. *IEEE Transactions on Neural Systems and Rehabilitation Engineering*, *14*, 5–13.

Schiefer, M. A., Triolo, R. J., & Tyler, D. J. (2008). A model of selective activation of the femoral nerve with a flat interface nerve electrode for a lower extremity neuroprosthesis. *IEEE Transactions on Neural Systems and Rehabilitation Engineering*, *16*, 195–204.

Shannon, R. V. (1992). A model of safe levels for electrical stimulation. *IEEE Transactions on Biomedical Engineering*, *39*, 424–426.

Shannon, R. V. (2012). Advances in auditory prostheses. *Current Opinion in Neurology*, *25*, 61–66. http://dx.doi.org/10.1097/WCO.0b013e32834ef878.

Silver, J., & Miller, J. H. (2004). Regeneration beyond the glial scar. *Nature Reviews Neuroscience*, *5*, 146–156.

Smart, S. K., Cassady, A. I., Lu, G. Q., & Martin, D. J. (2006). The biocompatibility of carbon nanotubes. *Carbon*, *44*, 1034–1047.

Stroncek, J. D., & Reichert, W. M. (2007). Overview of wound healing in different tissue types. In W. M. Reichert (Ed.), *Indwelling neural implants: Strategies for contending with the in vivo environment*. Boca Raton: CRS Press.

Struijk, J. J., Holsheimer, J., & Boom, H. B. (1993). Excitation of dorsal root fibers in spinal cord stimulation: a theoretical study. *IEEE Transactions on Biomedical Engineering*, *40*, 632–639.

Sunderland, S. (1991). Nerve grafting and related methods of nerve repair. In *Nerve injuries and their repair: A critical appraisal* (pp. 467–497). Edinburgh: Churchill Livingstone.

Sweeney, J. D., Ksienski, D. A., & Mortimer, J. T. (1990). A nerve cuff technique for selective excitation of peripheral nerve trunk regions. *IEEE Transactions on Biomedical Engineering*, *37*, 706–715.

Sweeney, J., Mortimer, J., & Durand, D. (1987). Modeling of mammalian myelinated nerve for functional neuromuscular stimulation. In *IEEE ninth annual conference of the engineering in medicine and biology society* (pp. 1577–1578).

Szarowski, D. H., Andersen, M. D., Retterer, S., Spence, A. J., Isaacson, M., Craighead, H. G., et al. (2003). Brain responses to micro-machined silicon devices. *Brain Research*, *983*, 23–35.

Taylor, R. S., Desai, M. J., Rigoard, P., & Taylor, R. J. (2013). Predictors of pain relief following spinal cord stimulation in chronic back and leg pain and failed back surgery syndrome: a systematic review and meta-regression analysis. *Pain Practice*.

Turner, J. N., Shain, W., Szarowski, D. H., Andersen, M., Martins, S., Isaacson, M., et al. (1999). Cerebral astrocyte response to Micromachined silicon implants. *Experimental Neurology*, *156*, 33–49.

Velasco, M., Velasco, F., & Velasco, A. L. (2001). Centromedian-thalamic and hippocampal electrical stimulation for the control of intractable epileptic seizures. *Journal of Clinical Neurophysiology*, *18*, 495–513.

Wadhwa, R., Lagenaur, C. F., & Cui, X. T. (2006). Electrochemically controlled release of dexamethasone from conducting polymer polypyrrole coated electrode. *Journal of Controlled Release*, *110*, 531–541.

Wang, Q., Millard, D. C., Zheng, H. J., & Stanley, G. B. (2012). Voltage-sensitive dye imaging reveals improved topographic activation of cortex in response to manipulation of thalamic microstimulation parameters. *Journal of Neural Engineering*, *9*, 026008.

Wei, X. F., & Grill, W. M. (2005). Current density distributions, field distributions and impedance analysis of segmented deep brain stimulation electrodes. *Journal of Neural Engineering*, *2*, 139–147.

Wei, X. F., & Grill, W. M. (2009). Impedance characteristics of deep brain stimulation electrodes in vitro and in vivo. *Journal of Neural Engineering*, *6*, 046008.

Weiner, R. L., & Reed, K. L. (1999). Peripheral Neurostimulation for control of intractable occipital neuralgia. *Neuromudulation: Technology at the Neural Interface*, *2*, 217–221.

Yang, J., Kim, D. H., Hendricks, J. L., Leach, M., Northey, R., & Martin, D. C. (2005). Ordered surfactant-templated poly(3,4-ethylenedioxythiophene) (PEDOT) conducting polymer on microfabricated neural probes. *Acta Biomaterialia*, *1*, 125–136.